

Discovery of (+)-*N*-(3-Aminopropyl)-*N*-[1-(5-benzyl-3-methyl-4-oxo-[1,2]thiazolo[5,4-*d*]pyrimidin-6-yl)-2-methylpropyl]-4-methylbenzamide (AZD4877), a Kinesin Spindle Protein Inhibitor and Potential Anticancer Agent

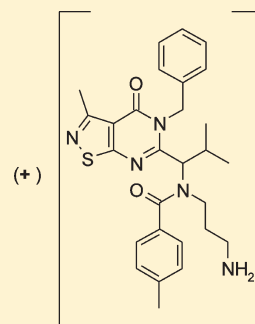
Maria-Elena Theoclitou,^{*,†} Brian Aquila,[†] Michael H. Block,[†] Patrick J. Brassil,[†] Lillian Castriotta,[†] Erin Code,[†] Michael P. Collins,[†] Audrey M. Davies,[†] Tracy Deegan,[†] Jayachandran Ezhuthachan,^{†,§} Sandra Filla,^{†,||,§} Ellen Freed,^{†,§,⊥} Haiqing Hu,[†] Dennis Huszar,[†] Muthusamy Jayaraman,[#] Deborah Lawson,[†] Paula M Lewis,[†] Murali V. P. Nadella,[†] Vibha Oza,[†] Maniyan Padmanilayam,[#] Timothy Pontz,[†] Lucienne Ronco,^{†,§} Daniel Russell,[†] David Whitston,[†] and Xiaolan Zheng[†]

[†]Cancer & Infection Research Area, AstraZeneca, Alderley Park, Macclesfield, Cheshire, SK10 4TG, United Kingdom

[‡]Cancer & Infection Research Area, AstraZeneca R&D Boston, 35 Gatehouse Drive, Waltham, Massachusetts 02451, United States

S Supporting Information

ABSTRACT: Structure–activity relationship analysis identified (+)-*N*-(3-aminopropyl)-*N*-[1-(5-benzyl-3-methyl-4-oxo-[1,2]thiazolo[5,4-*d*]pyrimidin-6-yl)-2-methylpropyl]-4-methylbenzamide (AZD4877), from a series of novel kinesin spindle protein (KSP) inhibitors, as exhibiting both excellent biochemical potency and pharmaceutical properties suitable for clinical development. The selected compound arrested cells in mitosis leading to the formation of the monopolar spindle phenotype characteristic of KSP inhibition and induction of cellular death. A favorable pharmacokinetic profile and notable in vivo efficacy supported the selection of this compound as a clinical candidate for the treatment of cancer.



First generation antimetabolic drugs, such as taxanes and vinca alkaloids, have demonstrated single-agent activity and also form the basis for a number of established combination therapies in cancer therapy.¹ Agents of this type exhibit a broad range of clinical effectiveness by disrupting spindle dynamics, leading to mitotic arrest and apoptosis.^{2,3} While effective, these drugs also have significant toxicological limitations. Microtubules are vital in nonproliferating cells, required for such processes as cell signaling and vesicular transport, thus tubulin-targeting agents often demonstrate toxicities such as neurotoxicity and peripheral neuropathy.^{4,5} Furthermore, innate and acquired resistance is a significant limitation of current therapies due to tumor cells becoming resistant to microtubule poisons through a variety of mechanisms, inclusive of tubulin mutations.^{6–8} A clinical opportunity hence exists for novel antimetabolic approaches that are more specific and have the potential to overcome observed toxicities and mechanisms of resistance commonly seen with microtubule targeting drugs.

Mitotic kinesins have gained significant attention as new targets for cancer therapy. Mitotic kinesins are molecular motor proteins which are essential for the assembly and function of the mitotic spindle.^{9–12} 623 kinesins have been identified to date, and these have been categorized into 14 different families. Kinesin spindle protein (KSP) or HsEg5 (*Homo sapiens* Eg5)^{10,13,14} is a member of the *bimC* subfamily of kinesin related

proteins. The expression profile of KSP is indicative of its role in mitosis. KSP is expressed in the thymus, tonsils, testes and bone marrow and is absent from human central nervous system neurons, which are postmitotic.¹¹ Negligible levels of KSP are detectable in adult nonproliferating tissue, while expression is prominent in proliferating tissue during development.^{14–16} The only known postdevelopment role for KSP is in the prophase of mitosis, where it is required for centrosome separation and the formation of a bipolar mitotic spindle.^{10,17} Inhibition of KSP in proliferating tumor cells results in inhibition of centrosome separation and consequent formation of a monopolar, or monoastal, spindle,^{10,18} arresting cells in mitosis and ultimately leading to cell death. Since KSP inhibition has no apparent effect on microtubules in nondividing cells, KSP inhibitors are not expected to cause peripheral neuropathy, a side effect attributed to disruption of the neuronal tubulin network.¹⁹ KSP is also not expressed in the adult central/peripheral nervous system,¹¹ consequently limiting the central nervous system side effect profile of its inhibitors.

In addition, overexpression of KSP levels has been observed in a variety of human solid tumors, inclusive of breast, lung, ovarian,

Received: May 18, 2011

Published: September 07, 2011

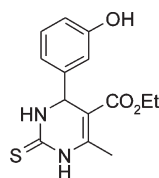


Figure 1. Structure of monastrol.

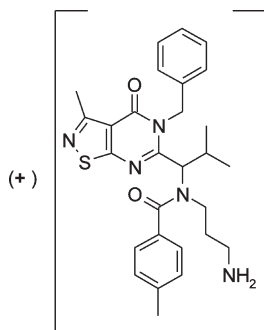


Figure 2. Structure of compound 1 (AZD4877).

colon and bladder cancers, and leukemias.^{20–22} However, this has often been observed in the context of a high mitotic index and corresponding increases in expression of other mitotic markers and may be primarily a reflection of a higher proliferative rate.^{20,21}

All of these observations render KSP a very attractive pharmacological target with the potential for inhibitors to exhibit broad spectrum antitumor efficacy, matched with improved tolerability, alongside activity in drug-resistant patient populations, compared to current microtubule focused agents.

Interest in mitotic kinesins as oncological drug targets was instigated by the initial identification of monastrol (Figure 1) as a selective KSP inhibitor.¹⁸ Since its discovery, a variety of potent KSP inhibitors have been reported that inhibit via an allosteric mode of inhibition (including SB-715992, SB-743921, CK010-6023, MK-0731, ARRY-520 and HR22C16-A1;^{23–37} the data on the large majority of these inhibitors have been published after the period during which the current work described within this paper was conducted). These inhibitors block enzymatic and cellular functions resulting in decreased cellular proliferation, mitotic arrest and cell death.²⁸ SB-715992, CK0106023, MK-0731 and HR22C16-A1 have all been shown to possess antitumor activity in xenograft models of cancer.^{30,31,35–40} KSP inhibitors remain effective in tumor cells resistant to paclitaxel, as recent results have also demonstrated.^{28,39}

Herein we describe the discovery of a class of potent, selective inhibitors of KSP, from which was derived our ultimate compound. Compound 1 (AZD4877)^{41,42} (Figure 2) exhibits favorable pharmacokinetic parameters and activity in a pharmacodynamic model consistent with a potential therapeutic role in the treatment of neoplastic disease.

CHEMISTRY

From extensive analysis of the sparse KSP inhibition literature information available at the time of project commencement,⁴³ the initial aim of the chemistry effort was to synthesize KSP inhibitors of the nature shown in Figure 3 in order to obtain structure–activity relationships at the various positions of diversity around the central fused pyrimidinone core. No generic

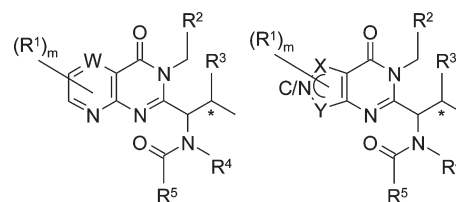


Figure 3. Modifications to five and six membered scaffolds examined (R^1 – R^5).

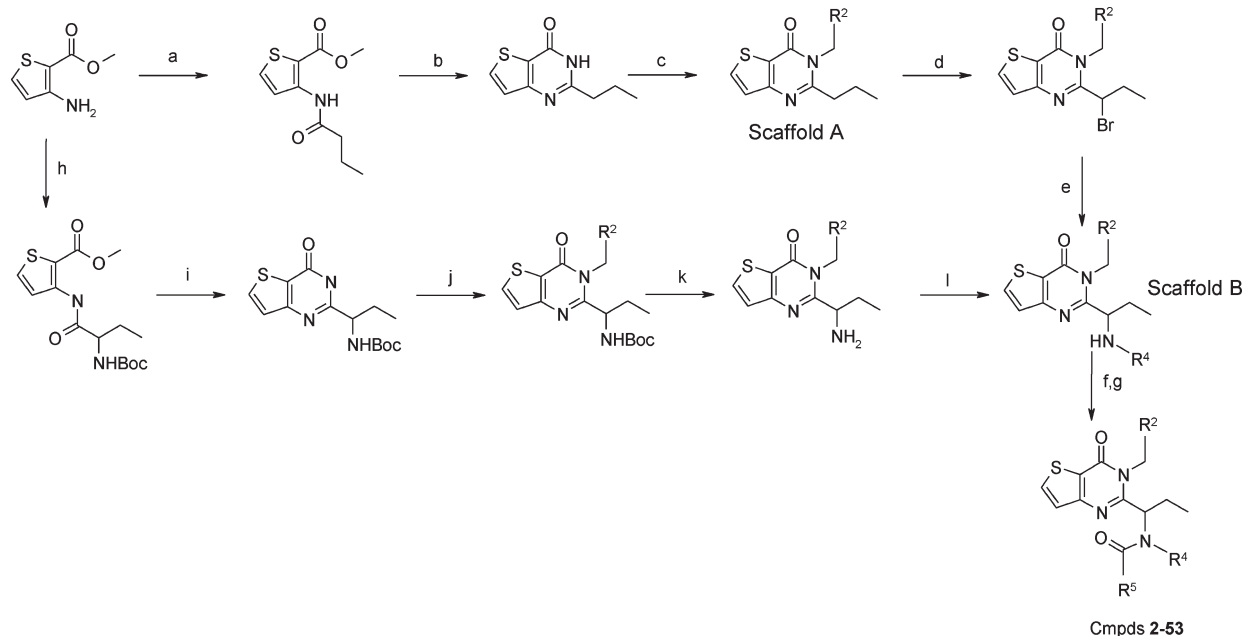
synthesis could be used to obtain the large diversity of fused core scaffolds necessary and hence each intermediate synthetic route is outlined separately.

The main preparation of compounds 2–53, containing the 3*H*-thieno[2,3-*e*]pyrimidin-4-one core, is outlined in Scheme 1. Methyl 3-aminothiophene-2-carboxylate was acylated to generate methyl 3-(butanoylamino)thiophene-2-carboxylate (step a), which subsequently underwent cyclization (step b), followed by alkylation (step c) with the respective R^2 diverse reagents to yield scaffold A. Subsequent bromination of these compounds (step d) gave yield to the intermediates desired. These compounds were then converted into the desired final compounds (compounds 2–53) via bromide displacement (with the desired R^4 diverse amines (step e)) and acylation (step f), to ultimately include the respective R^5 moiety. Final products were obtained via deprotection, if necessary.

Intermediate compounds of the nature of scaffold B (which ultimately would lead to generation of compounds 2–53) could also be obtained via a parallel route (Scheme 1). This route namely involved coupling of methyl 3-aminothiophene-2-carboxylate (same starting material used to generate scaffold A) with 2-[(2-methylpropan-2-yl)oxycarbonylamino]butanoic acid (step h), followed by cyclization (step i) and alkylation with the desired R^2 diverse reagents (step j). Final deprotection (step k) and reductive amination (step l) with the respective aldehydes (incorporating R^4 diversity) resulted in scaffold B, which could be converted, as previously, to the final desired compounds via acylation (incorporating R^5 diversity (step f)) and deprotection (step g, if required).

Schemes 2 and 3 outline the synthetic procedures used to generate compounds 54–61, 63, 64 (containing variations to the heterocyclic core). The furan scaffold analogue was generated via Scheme 2 (steps 1a–1j). Furan-3-carboxylic acid was reacted under Curtius conditions to generate *N*-furan-3-ylbutanamide (steps 1a, 1b). Vilsmeier–Haack reaction (step 1c) followed by conversion of the resultant aldehyde into the cyano analogue (step 1d), cyclization (step 1e) and subsequent benzylation ($R^2 = (\text{Ph})$) (step 1f) yielded scaffold C. Conversion into the desired final compound was accomplished in a similar manner to the analogue outlined in Scheme 1, namely, bromination, introduction of R^4 via amine displacement ($R^4 = -(\text{CH}_2)_3\text{NHBoc}$), acylation to introduce R^5 ($R^5 = (4\text{-Me Ph})$) and final protecting group removal to yield compound 54 (steps 1g–1j).

The pyrrole analogue scaffold was produced via Scheme 2 (steps 2a–2k). Isoxazole was reacted with diethyl 2-aminopropanedioate to generate ethyl 3-amino-1*H*-pyrrole-2-carboxylate (step 2a). Acylation, cyclization and subsequent benzylation ($R^2 = (\text{Ph})$) offered scaffold D (steps 2b–2e). Application of the same procedure as Scheme 2 (step 1g) led to bromination of the five membered heterocyclic ring only. Utilization of a different bromination procedure (Scheme 2, step 2g) allowed the introduction of bromide in the desired position. Introduction

Scheme 1. Synthesis of Compounds Containing 3*H*-Thieno[2,3-*e*]pyrimidin-4-one Core (Compounds 2–53)^a

^a Conditions: (a) butanoyl chloride, CH_2Cl_2 , Et_3N , 0°C , 30 min (99%); (b) NH_4OH , pressure reactor, 105°C , 3 h (70%); (c) $\text{R}^2\text{CH}_2\text{Br}$, K_2CO_3 , DMF, 25°C , 12 h; (d) Br_2 , NaOAc , AcOH , 55°C , 30 min; (e) R^4NH_2 , K_2CO_3 , DMF, 55°C , 1 h; (f) R^5COCl , CH_2Cl_2 , Et_3N , 25°C , 30 min; (g, if required) TFA, CH_2Cl_2 , 25°C , 30 min; (h) CH_2Cl_2 , 1-ethyl-3-(3-dimethylaminopropyl)carbodiimide hydrochloride, *N*-ethyl-*N*-propan-2-ylpropan-2-amine, DMAP, rt, 48 h (74%); (i) 30% NH_4OH , 95°C , 2 h (50%); (j) $\text{R}^2\text{CH}_2\text{Cl}$, K_2CO_3 , DMF, rt, 16 h; (k) HCl, dioxane, rt, 2 h; (l) *tert*-butyl *N*-(3-oxopropyl)carbamate, $\text{C}_2\text{H}_4\text{Cl}_2$, Et_3N , rt, 30 min then sodium triacetoxyborohydride rt, 1 h.

of R^4 was achieved via amine displacement ($\text{R}^4 = -(\text{CH}_2)_3\text{-NH}(\text{Boc})$) (step 2h), and acylation introduced R^5 ($\text{R}^5 = (4\text{-Me Ph})$) (step 2i). Dehalogenation of the heterocyclic ring was carried out prior to final protecting group removal to generate compound **55** (steps 2j, 2k).

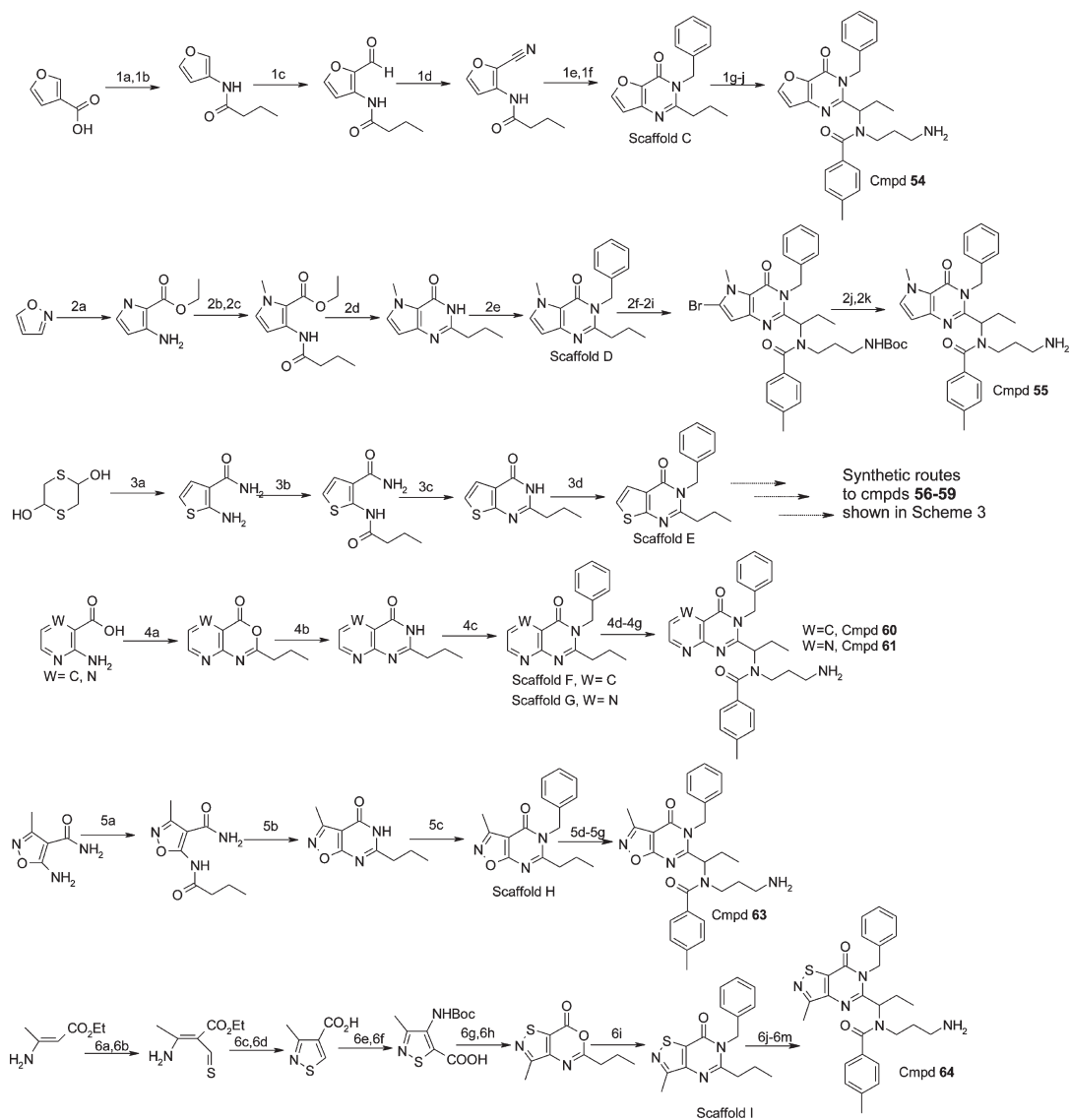
Synthesis of substituted analogues of 3*H*-thieno[3,2-*e*]pyrimidin-4-one was accomplished in a similar manner, and the main scaffold synthesis is shown in Scheme 2 (steps 3a–3d). Starting materials 1,4-dithiane-2,5-diol and 2-cyanoacetamide were utilized to generate 2-aminothiophene-3-carboxamide (step 3a), which was then acylated, cyclized and benzylated ($\text{R}^2 = (\text{Ph})$) to give the intermediate scaffold E (steps 3b–3d). The synthetic routes for compounds **56**–**59** are shown fully in Scheme 3. Bromination of scaffold E led to a dibrominated intermediate (Scheme 3, steps a, b). This compound was progressed via amine displacement (R^4 introduction; $\text{R}^4 = -(\text{CH}_2)_3\text{NH}(\text{Boc})$) and acylation (R^5 introduction, $\text{R}^5 = (4\text{-Me Ph})$) (steps c, d) and subsequently generated compounds **56** (via deprotection) (step e) and **57** (via dehalogenation followed by deprotection) (steps f, g). Chiral purification of **56** generated **66** and **67**. Scaffold E also served to generate **58** and **59**. Chlorination of scaffold E followed by bromination led to a mixture of compounds shown in Scheme 3 (steps h, i). Progression of this mixture via amine displacement (R^4 introduction; $\text{R}^4 = -(\text{CH}_2)_3\text{NH}(\text{Boc})$), acylation (R^5 introduction, $\text{R}^5 = (4\text{-Me Ph})$) and deprotection ultimately gave yield to **58** and **59** (steps j–l).

The six membered ring analogues were synthesized via cyclic oxazinones. Namely, in Scheme 2 (steps 4a–4c), 2-aminopyridine-3-carboxylic acid ($\text{W} = \text{C}$) was acylated and converted into the oxazinone, before being converted into the desired

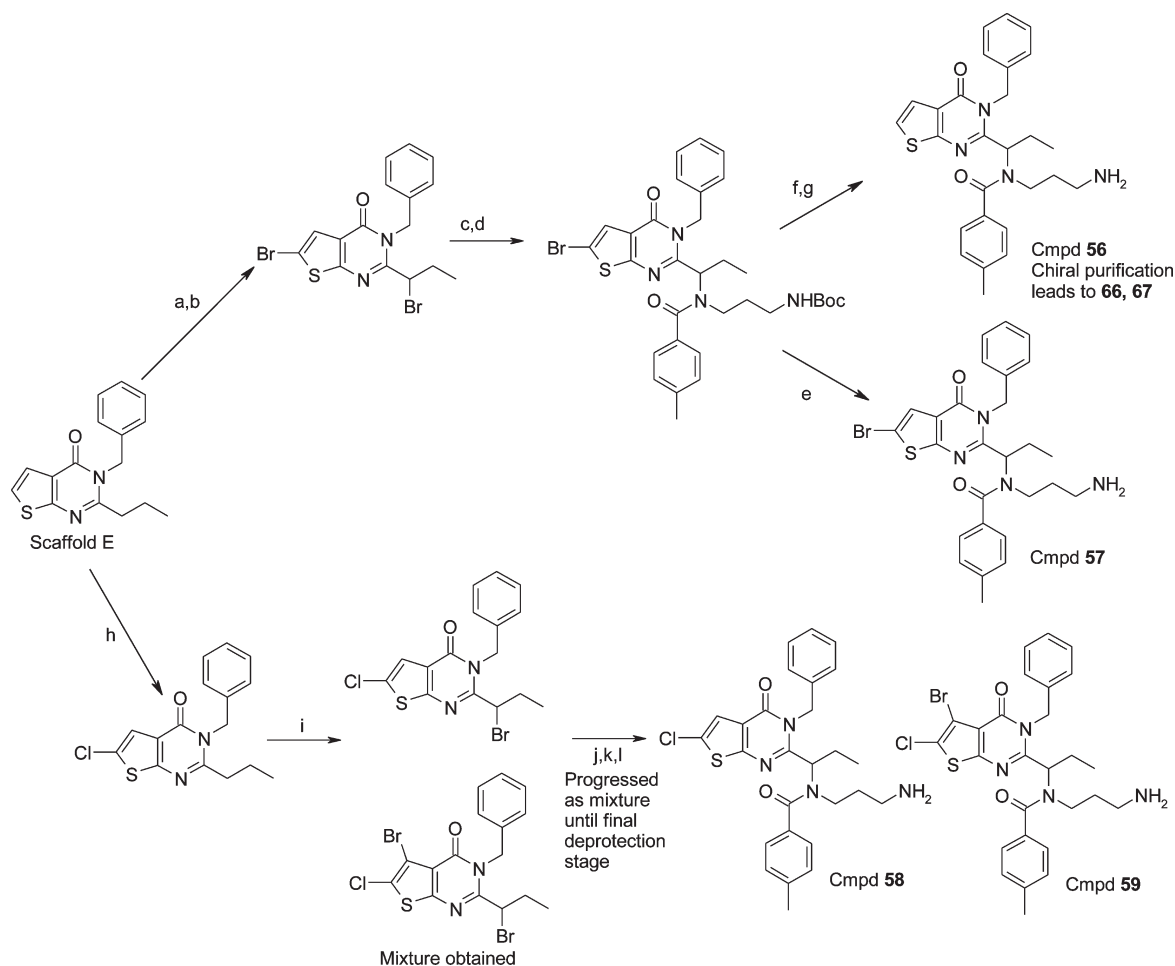
quinazolinone analogue (scaffold F ($\text{R}^2 = (\text{Ph})$)). The 3-amino-pyrazine-2-carboxylic acid analogue compound ($\text{W} = \text{N}$) was generated in an identical fashion (scaffold G ($\text{R}^2 = (\text{Ph})$)). The terminal desired compounds were produced via similar reactions to those mentioned previously (steps 4d–4g), incorporating R^4 ($\text{R}^4 = -(\text{CH}_2)_3\text{NH}(\text{Boc})$) and R^5 ($\text{R}^5 = (4\text{-Me Ph})$), to produce **60** ($\text{W} = \text{C}$) and **61** ($\text{W} = \text{N}$) respectively.

The isoxazole scaffold analogue (scaffold H) was generated via synthesis of 5-(butanoylamino)-3-methyl-1,2-oxazole-4-carboxamide from commercially available starting materials (Scheme 2 (step 5a)). Cyclization and benzylation ($\text{R}^2 = (\text{Ph})$) gave yield to scaffold H (Scheme 2 (steps 5b, 5c)), which was ultimately converted to the final desired product **63** via similar steps to those mentioned previously ($\text{R}^4 = -(\text{CH}_2)_3\text{NH}(\text{Boc})$, $\text{R}^5 = (4\text{-Me Ph})$) (steps 5d–5g).

Synthesis of *N*-(3-aminopropyl)-*N*-[1-(6-benzyl-3-methyl-7-oxo-[1,2]thiazolo[4,5-*d*]pyrimidin-5-yl)propyl]-4-methylbenzamide (**64**) (Scheme 2 (steps 6a–6m)) was lengthy. Ethyl 3-amino-2-methanethiylbut-2-enoate was used to generate ethyl 3-methyl-1,2-thiazole-4-carboxylate (steps 6a, 6b), which was subsequently converted to 3-methyl-1,2-thiazole-4-carboxylic acid (steps 6c, 6d). Employment of the Curtius reaction led to synthesis of *tert*-butyl *N*-(3-methyl-1,2-thiazol-4-yl)carbamate (step 6e), which was then converted to 3-methyl-4-[(2-methylpropan-2-yl)oxycarbonylamino]-1,2-thiazole-5-carboxylic acid (step 6f). This compound was deprotected and converted to 3-methyl-5-propyl-[1,2]thiazolo[4,5-*d*][1,3]oxazin-7-one (steps 6g, 6h), by the use of butanoyl chloride. Reaction with benzylamine (step 6i) gave yield to scaffold I ($\text{R}^2 = (\text{Ph})$) and subsequent steps as

Scheme 2. Synthesis of Compounds Containing Variations to the Heterocyclic Core^a

^a Conditions: (1a) toluene, Et₃N, diphenylphosphoryl azide, 5–10 °C, 30 min, reflux 3 h; (1b) propyl magnesium chloride, 0–5 °C, 1 h (two steps 35%); (1c) POCl₃, DMF, 0–5 °C, 1.5 h (68%); (1d) NH₂OH, 4-methylbenzenesulfonic acid, MgSO₄, 55 °C, 16 h (77%); (1e) KOH, *t*-BuOH, reflux, 3 h (60%); (1f) bromomethylbenzene, K₂CO₃, tetrabutylammonium hydrogen sulfate, toluene, rt, 3 h, (61%); (1g) Br₂, NaOAc, AcOH, 50 °C, 30 min (88%); (1h) *tert*-butyl *N*-(3-aminopropyl)carbamate, Et₃N, CH₂Cl₂, 25 °C, 5 days (99%); (1i) 4-methylbenzoyl chloride, Et₃N, CH₂Cl₂, 25 °C, 30 min (93%); (1j) TFA, CH₂Cl₂, 25 °C, 30 min (67%); (2a) diethyl aminomalonate hydrochloride, EtOH, NaOEt, 8 °C, 30 min, then acetic acid, NaOAc, 25 °C, 48 h (38%); (2b) butanoyl chloride, CHCl₃, pyridine, 0 °C, 1 h (97%); (2c) benzyltributylammonium bromide, (CH₃)₂SO₄, CH₂Cl₂, 50% NaOH, 0–25 °C, 1 h (84%); (2d) 30% NH₄OH, 110–115 °C, 6 h (19%); (2e) K₂CO₃, toluene, tetrabutylammonium hydrogen sulfate, reflux, 16 h (both *N*- and *O*-benzylated products obtained); (2f) Br₂, NaOAc, AcOH, 65 °C, 5 min (96%); (2g) CCl₄, *N*-bromosuccinimide, 2,2'-azobisisobutyronitrile, reflux, 45 min (95%); (2h) *tert*-butyl *N*-(3-aminopropyl)carbamate, Et₃N, CH₂Cl₂, 25 °C, 5 days (36%); (2i) 4-methylbenzoyl chloride, Et₃N, CH₂Cl₂, 25 °C, 12 h (90%); (2j) 5% Pd/C, H₂, EtOH, 25 °C, 18 h (53%); (2k) TFA, CH₂Cl₂, 25 °C, 30 min (86%); (3a) 2-cyanoacetamide, EtOH, Et₃N, 50 °C, 3 h (72%); (3b) butanoyl chloride, CH₂Cl₂, Et₃N, 25 °C, 12 h (96%); (3c) 2 N NaOH, reflux, 1 h (88%); (3d) bromomethylbenzene, K₂CO₃, DMF, 25 °C, 12 h (62%); (4a) butanoyl butanoate, reflux, 1 h (W = C 64%, W = N 59%); (4b) 30% NH₄OH, 100 °C, 18 h (W = C 80%, W = N 52%); (4c) bromomethylbenzene, K₂CO₃, DMF, 25 °C, 12 h (both *N*- and *O*-benzylated products obtained); (5a) butanoyl butanoate, 150 °C, 0.5–1 h (87%); (4d) Br₂, NaOAc, AcOH, 45 °C, 30 min; (4e) *tert*-butyl *N*-(3-aminopropyl)carbamate, K₂CO₃, DMF, 60 °C, 4 h; (4f) 4-methylbenzoyl chloride, CH₂Cl₂, Et₃N, 25 °C; (4h) TFA, CH₂Cl₂, 25 °C, 30 min; (5b) 2 N aq NaOH, microwave, 140 °C, 20 min (74%); (5c) bromomethylbenzene, K₂CO₃, DMF, 25 °C, 16 h (68%); (5d) Br₂, NaOAc, AcOH, 100 °C, 48 h (62%); (5e) *tert*-butyl *N*-(3-aminopropyl)carbamate, K₂CO₃, CH₃CN, 100 °C, 16 h (74%); (5f) 4-methylbenzoyl chloride, CH₂Cl₂, Et₃N, 25 °C, 1 h (76%); (5g) HCl, dioxane, 25 °C, 2 h (93%); (6a) POCl₃, DMF, THF, 0 °C, 30 min; (6b) NaSH, CH₂Cl₂, rt (steps 6a and 6b, 74%); (6c) 3-chlorobenzenecarboxylic acid, EtOH, 75 °C, 2 h (93%); (6d) aq NaOH, THF, rt, 16 h (79%); (6e) *t*-BuOH, Et₃N, diphenylphosphoryl azide, reflux, 16 h (97%); (6f) LDA/THF, –78 °C, 4 h, then CO₂, rt, 16 h (39%); (6g) HCl, dioxane, rt, 16 h (100%) (6 h) butanoyl chloride, pyridine, 0 °C to rt, 16 h, then 2 M HCl (64%); (6i) phenylmethanamine, microwave, 200 °C, 20 min (71%); (6j) Br₂, NaOAc, AcOH, 100 °C, 30 min (99%); (6k) *tert*-butyl *N*-(3-aminopropyl)carbamate, *N*-ethyl-*N*-propan-2-ylpropan-2-amine, DMF, rt, 1 h; (6l) 4-methylbenzoyl chloride, CHCl₃, *N*-ethyl-*N*-propan-2-ylpropan-2-amine, 60 °C, 12 h; (6m) HCl, dioxane, rt, 30 min (steps k, l, m 16%).

Scheme 3. Synthesis of Compounds 56–59^a

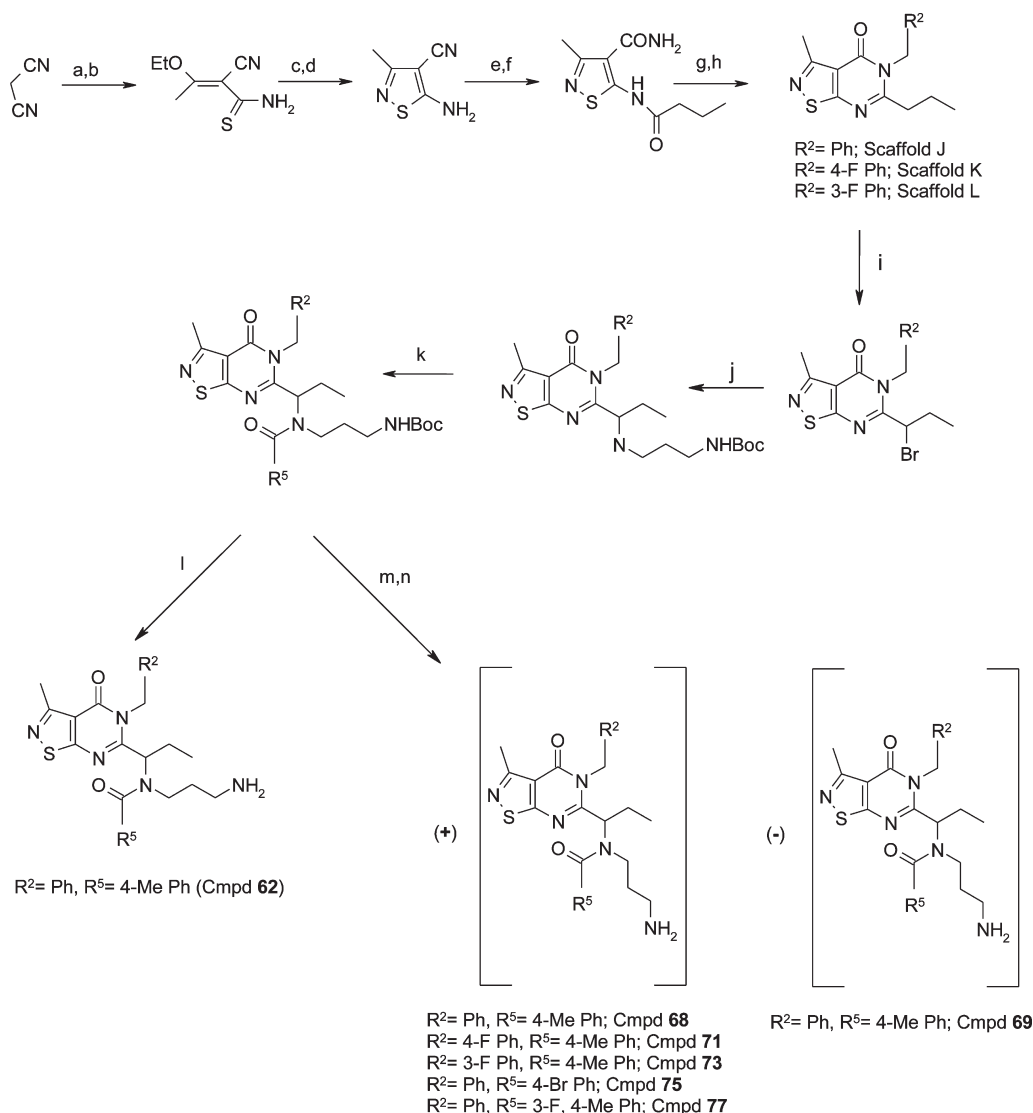
^a Conditions: (a) Br₂, NaOAc, AcOH, 45 °C, 30 min (60%); (b) Br₂, NaOAc, AcOH, 55 °C, 19.5 h (81%); (c) *tert*-butyl *N*-(3-aminopropyl)carbamate, K₂CO₃, DMF, 60 °C, 4 h (53%); (d) 4-methylbenzoyl chloride, CH₂Cl₂, Et₃N, 25 °C, 3 h (93%); (e) TFA, CH₂Cl₂, 25 °C, 30 min (96%); (f) 5% Pd/C, H₂, MeOH, 25 °C, 2.5 h (28%); (g) TFA, CH₂Cl₂, 25 °C, 30 min (98%); (h) *N*-chlorosuccinimide, DMF, 50 °C, 3 days, then ice, 1 h (84%); (i) Br₂, NaOAc, AcOH, 55 °C, 19.5 h (progressed as mixture); (j) *tert*-butyl *N*-(3-aminopropyl)carbamate, K₂CO₃, DMF, 60 °C, 4 h (mixture); (k) 4-methylbenzoyl chloride, CH₂Cl₂, Et₃N, 25 °C, 3 h (mixture); (l) TFA, CH₂Cl₂, 25 °C, 30 min (steps i–l: compound 58, 38%; compound 59, 23%).

outlined previously (steps 6j–6m) led to **64** (R⁴ = (–(CH₂)₃–NH(Boc)), R⁵ = (4-Me Ph)).

Scaffolds J, K and L (Scheme 4; R² = (Ph), (4-F Ph) and (3-F Ph) respectively) were synthesized from 5-amino-3-methyl-1,2-thiazole-4-carbonitrile via consecutive acylation (step e), conversion of the cyano moiety to an amide (step f), cyclization (step g) and finally benzylation (step h; R² = (Ph), (4-F Ph) and (3-F Ph) respectively). Synthesis of this respective intermediate arose from the cyclization of (2*E*)-3-amino-2-cyanobut-2-enethioamide, which had been synthesized via its precursor (2*E*)-2-cyano-3-ethoxybut-2-enethioamide (steps c, d). 2-(1-Ethoxyethylidene)propanedinitrile, synthesized from commercial starting materials, had been utilized to generate this precursor (steps a, b). Scaffolds J, K and L were then brominated (step i), and R⁴ was introduced via amine displacement (step j; R⁴ = (–(CH₂)₃NH(Boc))). Acylation with a variety of desired acyl chlorides (step k) gave yield to **62** (following deprotection, step l) and **68**, **69**, **71**, **73**, **75**, **77** (following chiral purification and subsequent deprotection, steps m, n).

The synthetic route utilized to generate **1** and its respective analogues is outlined in Scheme 5. The route incorporated

the use of the same intermediate utilized to synthesize **62**, namely, 5-amino-3-methyl-1,2-thiazole-4-carbonitrile. After acylation with the appropriate reagent (step a, R³ = (Me)), this compound was converted to scaffolds M, N and O (Scheme 5; R² = (Ph), (4-F Ph) and (3-F Ph) respectively) via cyclization and benzylation with the appropriate reagent (steps b–d). Displacement of the bromide with the respective R⁴-substituted amine, as had been utilized previously for all compounds (Schemes 2–4), could not be exploited in this case as this procedure led to elimination. Another route was hence devised via the conversion of the intermediate bromide to the azide analogue (steps e, f). Staudinger reduction (step g) gave yield to the desired amine analogue, and subsequent reductive amination (step h; R⁴ = (–(CH₂)₃NH(Boc))) resulted in the intermediate Boc-protected amine. Once again, acylation with a variety of desired acyl chlorides (step i) gave yield to **65** (following deprotection, step j) and **1**, **70**, **72**, **74**, **76**, **78** (following chiral purification and subsequent deprotection, steps k, l).

Scheme 4. Synthesis of Compounds 62, 68, 69, 71, 73, 75, 77^a

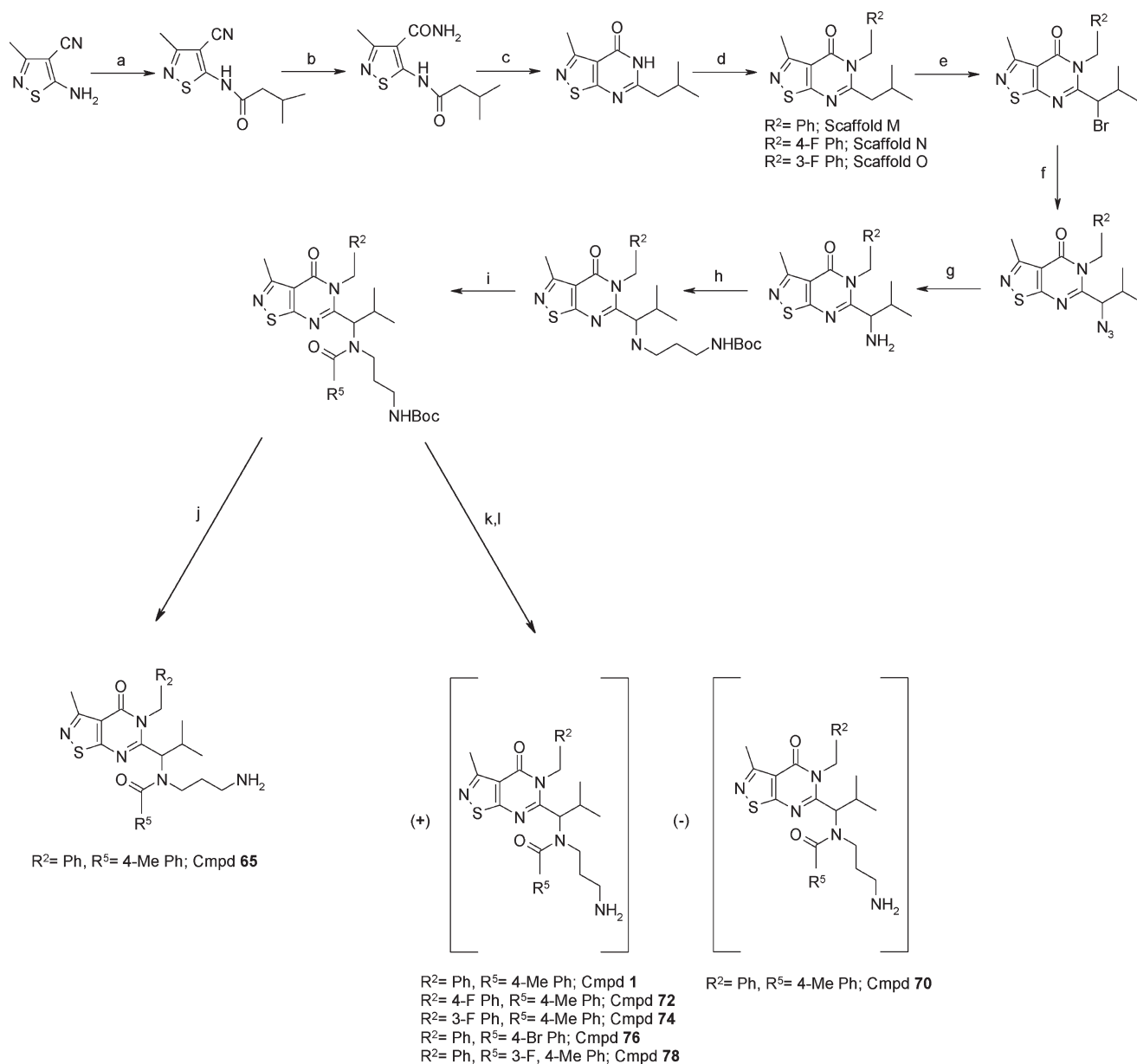
^a Conditions: (a) 1,1,1-triethoxyethane, glacial acetic acid, 85–140 °C, 40 min (91%); (b) H₂S, anhydrous benzene, Et₃N, rt 40 min (25%); (c) 30% NH₃/MeOH, 25 °C, 16 h (63%); (d) 30% hydrogen peroxide, MeOH, 60 °C, 4 h (80%); (e) butanoyl chloride, CH₂Cl₂, 25 °C, 16 h (95%); (f) 30% NH₃/MeOH, 30% hydrogen peroxide, 60 °C, 16 h (72%); (g) 30% NH₃/MeOH, 140 °C, 4 h (34%); (h) R²CH₂Br, K₂CO₃, DMF, 25 °C, 16 h (R² = Ph; 32%); (i) Br₂, NaOAc, AcOH, 100 °C, 20 min (R² = Ph; 100%); (j) *tert*-butyl *N*-(3-aminopropyl)carbamate, *N*-ethyl-*N*-propan-2-ylpropan-2-amine, EtOH, reflux, 16 h (R² = Ph; 17%); (k) R⁵COCl, CH₂Cl₂, Et₃N, 25 °C, 30 min (R² = Ph, R⁵ = 4-Me Ph; 94%); (l) HCl, ether, 25 °C, 20 h (R² = Ph, R⁵ = 4-Me Ph; 87%); (m) chiral purification (98% total recovery if respective enantiomers); (n) HCl, dioxane, rt, 20 min (100%).

RESULTS AND DISCUSSION

The separate positions of diversity were systematically varied around the central core to determine specific structure–activity relationships. Most potent compounds described showed clear cell cycle effects consistent with inhibition of KSP (monoastral phenotype observed).

Initially various alkylation substitutions were carried out on the *N*-(3-aminopropyl)-4-methyl-*N*-[1-(4-oxo-3*H*-thieno[3,2-*d*]pyrimidin-2-yl)propyl]benzamide scaffold (Table 1). Complete removal of the R² moiety rendered tested compounds with micromolar activity. The active site pocket appeared to be very spatially restricted in this area, as any minor substitution gave a decrease in activity (3 compared to 4–8); even the 2-fluoro-substituted analogue (4) resulted in significant changes in

activity. Ortho-substitutions were the most unfavorable (4), followed by para- and meta-position substitutions (6–8 and 5 respectively). Heterocyclic analogues (10–12) were less potent than their aryl counterparts presumably due to their decrease in topical lipophilicity. For example, replacement of the phenyl core with a pyridine core proved detrimental, regardless of the location of nitrogen (3 (nanomolar activity) compared to 10–12 (micromolar activity)). One example where the benzylic group was replaced with an alkyl moiety (9) also reduced potency (>75-fold decrease). Only the plain benzylic core (3) had accepted potency and resulted in appropriate cellular activity for compound progression. This site of modification (R²) was hence left unaltered for further exploratory work.

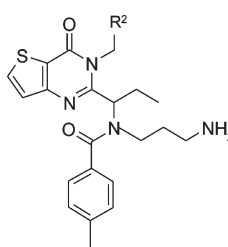
Scheme 5. Synthesis of Compounds 1, 65, 70, 72, 74, 76, 78^a

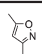
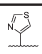
^a Conditions: (a) 3-methylbutanoyl chloride, pyridine, 0 °C to rt, 16 h (79%); (b) 30% NH_3/MeOH , hydrogen peroxide, 60 °C, 16 h (71%); (c) 30% NH_3/MeOH , 140 °C, 5 h (38%); (d) $\text{R}^2\text{CH}_2\text{Br}$, K_2CO_3 , DMF, rt, 16 h ($\text{R}^2 = \text{Ph}$; 70%); (e) Br_2 , NaOAc, AcOH, 100 °C, 50 min ($\text{R}^2 = \text{Ph}$; 99%); (f) NaN_3 , DMF, rt, 1 h ($\text{R}^2 = \text{Ph}$; 94%); (g) 5% Pd/C, H_2 , MeOH, rt (used without further purification); (h) *tert*-butyl *N*-(3-oxopropyl)carbamate, 4 Å molecular sieves, CH_2Cl_2 , rt, 3 h, then AcOH, sodium triacetoxyborohydride, rt, 16 h (used without further purification); (i) R^5COCl , CHCl_3 , pyridine, rt, 48 h (steps g, h and i ($\text{R}^2 = \text{Ph}$, $\text{R}^5 = 4\text{-Me Ph}$; 32%)); (j) HCl, dioxane, rt, 20 min ($\text{R}^2 = \text{Ph}$, $\text{R}^5 = 4\text{-Me Ph}$; 99%); (k) chiral purification ($\text{R}^2 = \text{Ph}$, $\text{R}^5 = 4\text{-Me Ph}$; 48%); (l) HCl, dioxane, rt, 20 min ($\text{R}^2 = \text{Ph}$, $\text{R}^5 = 4\text{-Me Ph}$; 100%).

Variation of the amine side chains rendered similar structure–activity relationships (Table 2) with complete removal of the amine side chain abolishing activity (15). The best side chain included a linear linker with a terminal primary amine, ideally with a three carbon length spacer (3 compared to 16). Fusions to yield secondary cyclic amine side chains (17–19) only served to give significant decreases in activity (3 compared to 17–19 resulted in >30–140-fold decrease), presumably due to steric interactions. Conversions of the terminal primary amine also decreased activity. A terminal amide (20), sulfonamide (21) or carbamate (22) moiety significantly reduced activity, yielding

micromolar compounds as a consequence. Hardly any amine side chain substitutions led to an increase in activity, hence no further significant R^4 changes were made to this linkage.

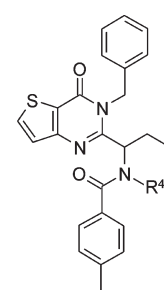
Distinct structure–activity relationships were obtained with substitutions of the pendant amide moiety (R^5 , Table 3). This pocket appeared to have a requirement for increased lipophilicity as well as necessitating certain structural requirements. Alkyl amide substitutions, whether acyclic (23, 24) or cyclic (25–27) resulted in micromolar activity. The effect of variation in lipophilicity was also seen with five membered heteroaromatic rings (45–47) as well as heteroaryl groups, such as substituted

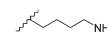
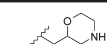
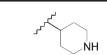
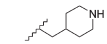
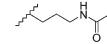
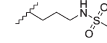
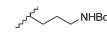
Table 1. Structure–Activity Relationships Resulting from Variation of R² (R³, R⁴ and R⁵ Are as Shown)


Cmpd number	R ²	Enzyme IC ₅₀ (μM)	Cell IC ₅₀ (μM)
2	Complete removal of CH ₂ R ²	9	
3	Ph	0.01	0.10
4	(2-F)Ph	0.14	1.36
5	(3-F)Ph	0.02	0.33
6	(4-Cl)Ph	0.21	1.56
7	(4-Me) Ph	0.13	0.65
8	(4-OMe) Ph	0.16	0.79
9	cyclopropyl	0.76	3.08
10	2-pyridyl	3.50	
11	3-pyridyl	3.80	
12	4-pyridyl	5.31	
13		0.63	1.71
14		9.09	

pyridine (48), which decreased potency significantly (compared to 3, compounds 45 and 47 resulted in >400-fold decrease whereas 46 and 48 resulted in ≥ 1000 -fold decrease). Bicyclic substitutions gave differing results (49–53). Bicyclics that served to reduce lipophilicity (49, 51) led to drastic decreases in activity. Compounds that retained lipophilicity (50) appeared to maintain activity with small activity variations arising from steric interactions.

The widest range of potency variations was observed with the monocyclic aryl moieties (Table 3, 28–44). The plain phenyl group (28) reduced activity (>200-fold decrease compared to 3), also presumably due to the decrease in lipophilicity. Common substitutions on the phenyl moiety rendered varying results. Substitution around the ring proved to be most detrimental in the ortho-position (29, 37) (>600-fold decrease compared to 3). Meta-substitution also served to decrease activity (compared to 3, compound 34 resulted in <10-fold decrease whereas 36 resulted in ≥ 300 -fold decrease). Electron withdrawing and electron donating groups in the para-position did affect the potency, however the activity observed appeared to be more correlated with the lipophilicity of the respective moieties (30, 32, 39). The positioning of a large lipophilic group in the para-position gave rise to the most potent compounds observed (3, 30, 32), presumably through the access of the distant section of this lipophilic pocket. Steric restrictions in this pocket led to a decrease in potency if larger lipophilic groups were employed (isopropyl, 40). The best

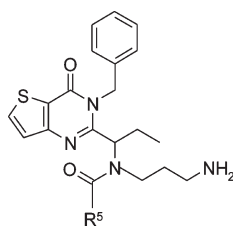
Table 2. Structure–Activity Relationships Resulting from Variation of R⁴ (R², R³ and R⁵ Are as Shown)


Cmpd number	R ⁴	Enzyme IC ₅₀ (μM)	Cell IC ₅₀ (μM)
15	H	9	
16		0.39	0.98
17		0.31	0.72
18		1.07	1.29
19		1.44	10
20		2.92	
21		5.99	
22		10	

activity was obtained when the para-position was substituted with either methyl (3) or bulky halogen substituents (30, 32).

The central fused pyrimidinone core was also varied to generate the large diversity of fused core final compounds necessary (Table 4). Compounds generated, with this variation (3, 54–64), contained the best moieties in positions R², R⁴ and R⁵ as identified previously (R² = Ph, R⁴ = $-(\text{CH}_2)_3\text{NH}_2$, R⁵ = 4-Me Ph). With regard to the respective fused heterocyclic scaffolds, in general, the six membered heterocyclic ring analogues (60, 61) exhibited lower potency than the five membered ring analogues (3, 54–59, 62–64). The lower potency was presumably due to the lower overall lipophilicity of the molecules synthesized.

Within the five membered heterocyclic ring series, compounds of the nature of 3, 54 and 55 (originating from scaffolds A, C and D respectively) all appeared to have similar potency, regardless of the five membered heterocyclic ring moiety present. In the thiophene series synthesized, compounds originating from scaffold E (56) were slightly more active than their regioisomeric counterparts originating from scaffold A (3). This was reflective more in their cellular potency rather than their enzyme potency. Substitutions with halogens at both the 2- and 3-positions of the compounds originating from scaffold E (57–59) decreased the overall potency from their unsubstituted analogue (56). This avenue was not investigated further. The most potent compounds from the five membered mono- or diheteroatom core variants (3, 54–64) were deemed to be 56, 62 and 63 (based on

Table 3. Structure–Activity Relationships Resulting from Variation of R⁵ (R², R³ and R⁴ Are as Shown)

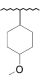
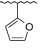
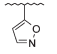
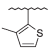
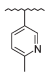
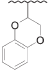
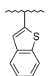
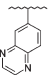
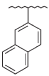
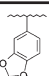
Cmpd number	R ⁵	Enzyme IC ₅₀ (μM)	Cell IC ₅₀ (μM)	Cmpd number	R ⁵	Enzyme IC ₅₀ (μM)	Cell IC ₅₀ (μM)
23	<i>n</i> -Butyl	5.52		39	4-EtPh	0.09	0.25
24	CH ₂ C(Me) ₂	4.54		40	4- <i>i</i> PrPh	0.94	3.3
25	Cyclopropyl	6.7		41	4-OMePh	0.21	0.64
26	Cyclopentyl	4.22		42	4-FPh	0.14	0.57
27		9		43	4-CNPh	2.70	
28	Ph	0.2	0.68	44	4-CO ₂ MePh	5.96	
29	2-ClPh	0.61	0.86	45		0.5	1.55
30	4-ClPh	0.05	0.20	46		1.39	
31	2,4-DiClPh	0.15	0.31	47		0.41	
32	4-BrPh	0.03	0.16	48		0.98	3.69
33	4-CF ₃ Ph	0.21	0.51	49		2.31	
34	3-CF ₃ Ph	0.31	0.58	50		0.04	
35	4-OCF ₃ Ph	2.46		51		3.21	
36	3-MePh	0.09	0.14	52		0.03	0.2
37	2-MePh	1.06		53		0.15	0.26
38	3-F, 4-MePh	0.02	0.06				

Table 4. Structure–Activity Relationships Resulting from Variation of the Fused Heterocyclic Core

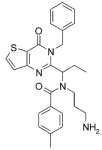
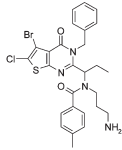
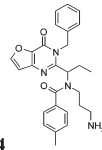
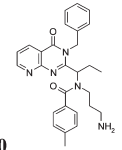
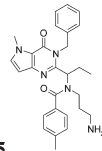
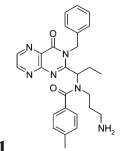
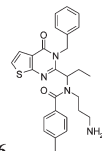
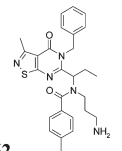
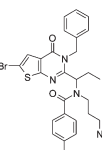
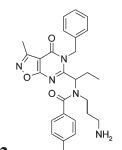
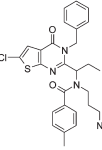
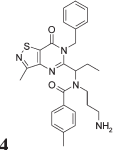
Cmpd	Enzyme IC ₅₀ (μ M)	Cell IC ₅₀ (μ M)	Cmpd	Enzyme IC ₅₀ (μ M)	Cell IC ₅₀ (μ M)
 3	0.012	0.104	 59	0.161	0.675
 54	0.013	0.174	 60	0.323	1.4
 55	0.021	0.043	 61	5.46	
 56	0.008	0.030	 62	0.003	0.004
 57	0.141	0.763	 63	0.016	0.023
 58	0.085	0.464	 64	0.005	0.045

Table 5. Solubility of Most Potent Compounds

compd	solubility (μ M)
56	1239
62	1572
63	69

a combination of their enzyme and cellular potency) and hence were progressed further to determine their respective physical properties and pharmacokinetic parameters, ultimately contributing to their in vivo efficacy.

The program goal was an intravenous (iv) agent, and hence aqueous solubility was vitally important. The solubility of the three initial leads chosen (**56**, **62**, **63**) was thus measured (Table 5). From the results outlined, the decision was made to

further progress only compounds **56** and **62** as these compounds exhibited millimolar solubility (compared to micromolar for **63**) and were thus better suited for the overall drug profile required.

The sole position of diversity that remained to be explored was R³ (Figure 2). The variation of this moiety was intentionally left to the latter stages for ease of synthesis. These compounds required an entirely different synthetic route to be devised (Scheme 5). R³ variation (R³ = (H) or (Me)) was thus restricted to the isothiazole scaffold, as this was indicated as the most promising core variation (from Table 5). Results (shown in Table 6) indicated that the newly synthesized compound **65** (R³ = (Me)) had very similar cellular potency to compound **62** (R³ = (H)) and hence a distinction would have to be made between **56**, **62** and **65** using further parameters to enable their progression.

From the overall data available (Tables 1–6), **56**, **62** and **65** stood out as the most potent and promising compounds for

progression to in vivo models. Due to the fact that these compounds were chiral in nature, they were subsequently separated into their respective enantiomers (**1**, **66–70**), and their enzyme and cellular activities are shown in Table 7. The most active enantiomer (**1**, **66**, **68**) was always the (+) antipode (when dissolved at a concentration of 1 mg/mL in methanol, at 20.0 °C measured at 589 nm). Based on the cellular potencies of the respective enantiomers, **62** and **65** were chosen for progression.

In order to further explore the isothiazole scaffold exhibited in compounds **62** and **65**, a distinct set of isothiazole compounds was synthesized, in parallel, encompassing the best variants identified at each R group position (Tables 1, 2, 3 and 6; R² = (Ph), (4-F Ph), (3-F Ph); R³ = (H), (Me); R⁴ = (–(CH₂)₃–NH₂); R⁵ = (4-Me Ph), (4-Br Ph), (3-F, 4-Me Ph)). All of these analogues were synthesized by incorporation of the desired R²–R⁵ groups into the respective steps outlined in Schemes 4 and 5. The final enantiomers were isolated for comparison (**71–78**), and their cellular potencies are shown in Table 8.

In order to determine the ultimate compounds for progression, combined enzyme and cellular data (outlined in Tables 7

and 8) were utilized, and a decision was made to further progress compounds **1** and **68** as the best candidates.

The lower in vivo clearance (nude mouse) of **1** in comparison to **68** (17 mL/min/kg vs 50 mL/min/kg; Table 9) served to aid the project in determining **1** as the ultimate compound to eventually progress into our pharmacodynamic model.

Prior to its assessment in our pharmacodynamic model to determine its in vivo efficacy, further analysis of its pharmacokinetic properties was carried out.

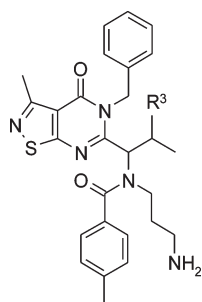
Cytochrome P450 (CYP450) Inhibition. The potential for **1** to inhibit human cytochrome P450s was assessed in vitro using specific substrates, recombinant enzymes and analysis by mass spectrometry. For all five human isoforms tested (CYP1A2, 2C9, 2C19, 2D6 and 3A4), IC₅₀ values obtained were >10 μM. The potential for a clinically significant effect of **1** on the disposition of other concomitant medications was hence considered low.

Kinesin and Kinase Selectivity. We were seeking to identify a small molecule inhibitor of KSP, which was selective in relation to other kinesins. To avoid nonspecific activity against other targets, the compound also had to be selective versus a diverse range of enzymes, receptors, ion channels and transporters, inclusive of kinases. The activity of **1** was hence evaluated against human recombinant KSP and two other selected kinesins in vitro. Mitotic kinesin-like protein (MKLP) and conventional kinesin were significantly less sensitive to **1**, exhibiting IC₅₀ values of 50 μM and IC₅₀ of >100 μM respectively.

In a separate panel, **1** (at a 10 μM concentration) did not significantly inhibit any of 25 kinases screened (confidential data). The highest inhibition was seen with lymphocyte specific protein tyrosine kinase (LCK) and mitogen-activated protein kinase-activated protein kinase 1a (MAPKAP-K1a) at 42% and 35% respectively.

1 was also tested in a panel of 62 in vitro radioligand binding and enzyme assays covering a diverse range of enzymes, receptors, ion channels and transporters at a single concentration of 10 μM (company: MDS Pharma Services, Lead Profiling Screen, available in the Supporting Information). Significant activity (defined as >50% inhibition) was detected in only 5 of the 62 in vitro radioligand binding and enzyme assays (namely, 5-lipoxygenase, somatostatin receptor 1, two sites of the L-type calcium

Table 6. Structure–Activity Relationships Resulting from Variation of R³



compd	R ³	cell IC ₅₀ (μM)
62	H	0.004
65	Me	0.002

Table 7. Enzyme and Cellular Potency of Respective Enantiomers (Compounds **1, **66–70**)**

Cmpd	Enzyme		Cmpd	Enzyme		Cmpd	Enzyme	
	IC ₅₀ (μM)	Cell IC ₅₀ (μM)		IC ₅₀ (μM)	Cell IC ₅₀ (μM)		IC ₅₀ (μM)	Cell IC ₅₀ (μM)
66 (+)	0.003	0.008	68 (+)	0.001	0.003	1 (+)	0.002	0.003
67 (-)	1.9		69 (-)	0.051		70 (-)	0.429	

Table 8. Distinct Set of Isothiazole Compounds, Encompassing the Best Variants at Each R²–R⁵ Group Position

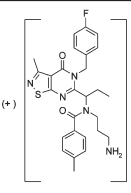
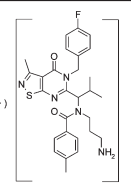
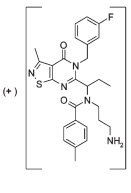
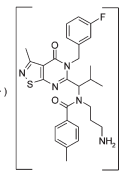
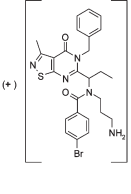
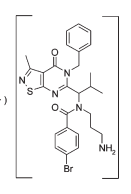
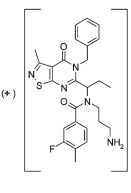
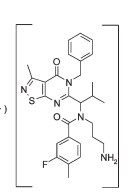
Cmpd	Cell IC ₅₀ (μM)	Cmpd	Cell IC ₅₀ (μM)
	0.105		0.019
71		72	
	0.013		0.005
73		74	
	0.014		0.006
75		76	
	0.012		0.010
77		78	

Table 9. In Vivo Clearance of Compounds 1 and 68

compd	nude mouse clearance (mL/min/kg)	compd	nude mouse clearance (mL/min/kg)
1	17	68	50

channel and also the sodium channel, Table 10). In follow-up studies, performed to explore the concentration–response relationship for **1** at these targets, the IC₅₀ for inhibition of the calcium channel activity (target: L-type calcium channel, guinea-pig ileum) was 2.7 μM and for the sodium channel (target: sodium channel, guinea-pig atria) was >30 μM. These values were several hundred fold above the enzyme IC₅₀ and hence were not likely to be pharmacologically meaningful.

Pharmacokinetics. Plasma protein binding was determined at 10 μM in both rat and human plasma by equilibrium dialysis and was considered to be high (95.4–95.6% bound; Table 11).

Compound **1** was incubated at 2 μM in rat liver microsomes and hepatocytes in order to determine the in vitro hepatic

Table 10. Effects of Compound 1 in in Vitro Enzyme and Radioligand Binding Assays^a

target	% inhibition at 10 μM of compd 1
sodium channel, site 2*	99
L-type calcium channel, benzothiazepine site*	87
somatostatin sst1 receptor	80
L-type calcium channel, phenylalkylamine site*	76
5-lipoxygenase	71

^a All human except where noted with an asterisk (*).

Table 11. Plasma Protein Binding of Compound 1

plasma	plasma protein binding (% bound)
rat (Wistar)	95.6
human	95.4

clearance. Intrinsic clearance (CL_{int}) values, predicted CL values and in vivo CL values are presented in Table 12.

In general, both microsomes and hepatocytes provided a reasonable prediction of total in vivo clearance for preclinical species tested.

The pharmacokinetic profile of **1** was assessed in rat following iv bolus dosing at 1 and 5 mg/kg. Clearance values were moderate in rat (50% of hepatic blood flow), and the volume of distribution was high (10 L/kg). The observed *t*^{1/2} (half-life) was 3.5 h.

The pharmacokinetic properties of **1** following a single iv bolus administration in rat are shown in Table 13.

In both male and female rats, the exposure of **1** was found to increase with increasing dose between 1 and 6 mg/kg. No differences in exposure were observed between day 1 and day 5 in a 5-day repeat dose study with single daily doses of 1 mg/kg.

Pharmacodynamic Activity in a Rat Hollow Fiber Model. Hollow fibers seeded with Colo205 cells were implanted subcutaneously into rats to assess the pharmacodynamic activity of **1**. Rats were treated with a single intravenous dose of the compound (6 mg/kg and 12 mg/kg) or vehicle. A statistically significant reduction in cell viability (Figures 4A and 5A–D) and increase in cleaved caspase 3 levels (data not shown) was seen by 48 h postdose at both dose levels. Increased numbers of monoasters were observed at both time points after treatment with **1** (Figures 4B and 5E,F), and the number of phospho-histone-H3 (PHH₃) positive cells was significantly increased at 24 h (Figures 4C and 5G,H). These observations are consistent with KSP inhibition and mitotic block resulting in cell death. Plasma levels of **1** were higher than that detected in fibers 2 h after dosing, but drug levels remained relatively constant in the fibers over 24 h resulting in higher levels than that detected in plasma (Figure 6). At the 6 mg/kg dose level this corresponded to a total average drug fiber concentration of 30.7 ng/mL (61 nM) and plasma concentration of 2.8 ng/mL (5.6 nM) 24 h postdose.

CONCLUSIONS

A series of novel, selective inhibitors of kinesin spindle protein have been exemplified. Compounds from this series have been shown to inhibit tumor cell growth in vitro with a mode of action that correlates with KSP inhibition. Structure–activity

Table 12. In Vitro Data Used To Predict in Vivo Clearance

species (sex)/strain	in vitro system	CL _{int} (μmol/min/mg) (μL/min/10 ⁶ cells)	predicted total		actual in vivo	
			hepatic CL (mL/min/kg)	% Q _h	CL (mL/min/kg)	% Q _h
rat (male)/Wistar	microsomes	<10	<14	<20	36	52
	hepatocytes	4–13	16–34	22–48		

Table 13. Pharmacokinetics of Compound 1 (Freebase) after a Single Iv Bolus Administration

species (strain)	dose (mg/kg)	AUC _{INF} (h ng/mL)	C ₀ (ng/mL)	CL (mL/min/kg)	t ^{1/2} (h)	V _{ss} (L/kg)
rat (Wistar)	6	2839	1076	36	3.5	10

relationship analysis identified **1** as exhibiting both excellent enzymatic and cellular potency. This compound exhibited a favorable pharmacokinetic profile and was progressed into pharmacodynamic studies in vivo. A rat hollow fiber model has shown that this compound displays activity consistent with KSP inhibition causing Colo 205 cells to form monoesters, block in mitosis and undergo cell death.

These findings supported the selection of **1** as a clinical candidate for the potential treatment of cancer. The safety, pharmacokinetics and efficacy of **1** have been assessed in phase I and II clinical trials in both solid and hematological tumors; the outcome of one of these trials has recently been reported.⁴⁴

EXPERIMENTAL SECTION

General Information. All solvents used were commercially available in anhydrous grade. Reagents were utilized without further purification unless otherwise stated. Organic solutions were dried over anhydrous sodium sulfate. Evaporation of solvent was carried out using a rotary evaporator under reduced pressure (600–4000 Pa (pascals); 4.5–30 mmHg) with a bath temperature of up to 60 °C. Solvent ratios are given in volume:volume (v/v) terms.

Temperatures are given in degrees Celsius (°C), and operations were carried out at room or ambient temperature, that is, at a temperature in the range of 18–30 °C.

In general, the course of reactions was followed by thin layer chromatography or mass spectroscopy and reaction times are given for illustration only; where a synthesis is described as being analogous to that described in a previous example, the amounts used are the millimolar ratio equivalents to those used in the previous example.

NMR data is in the form of delta values for major diagnostic protons, given in parts per million (ppm) relative to tetramethylsilane (TMS) as an internal standard, determined at 400 MHz using deuterated chloroform (CDCl₃) as solvent unless otherwise indicated.

Analytical mass spectra were run with an electron energy of 70 eV in the chemical ionization (CI) mode using a direct exposure probe; where indicated ionization was effected by electron impact (EI), electrospray (ESP), or atmospheric pressure chemical ionization (APCI); values for *m/z* are given; generally, only ions which indicate the parent mass are reported.

The purity of all final compounds was confirmed by analysis with an Agilent 1100 liquid chromatography unit (LC) with an Agilent 1100 mass spectroscopy detector (MSD) or a Waters ZQ mass spectrometer (compounds were detected by mass spectroscopy in APCI⁺ ionization) using a Luna 3μ C8 (2) column (100A, 30 × 2.0 mm), eluting with mixtures of water–acetonitrile (ranging from 5 to 98% acetonitrile/water

with 0.1% formic acid), using a UV detector at 220, 240, and 254 nm. The purity of all final compounds was ≥95%.

Chiral HPLC separation was carried out by comparison of the elution times of the compound with a 1:1 mixture of the racemate. The enantiomeric excess of the final compound was calculated using the area percent of the UV signal at 220 nm from chiral HPLC analysis.

The rotation parameters were measured by a Perkin-Elmer polarimeter 341. Measurements were made of compounds dissolved at a concentration of 1 mg/mL in methanol, at 20.0 °C measured at 589 nm.

The synthetic procedures for all compounds mentioned within the article are described, in extensive detail, in the accompanying Supporting Information. Final synthetic steps for certain key compounds (namely, compounds **1**, **62**, **65**, **68** and **71–78**) are outlined below (along with their respective method numbers).

Method 76. *N*-(3-Aminopropyl)-*N*-[1-(5-benzyl-3-methyl-4-oxo-[1,2]-thiazolo[5,4-*d*]pyrimidin-6-yl)propyl]-4-methylbenzamide Hydrochloride. *tert*-Butyl *N*-[3-[1-(5-benzyl-3-methyl-4-oxo-[1,2]-thiazolo[5,4-*d*]pyrimidin-6-yl)propylamino]propyl]carbamate (method 75) (0.117 g, 0.198 mmol) was dissolved in 2 M HCl in ether, and the mixture was stirred at rt for 20 h. The precipitated product was filtered off and washed with ether and dried in vacuo to yield the desired product (**62**) (0.091 g, 87%): ¹H NMR (DMSO-*d*₆ 300 MHz, 96 °C) δ 7.79 (bs, 3H), 7.37–6.95 (m, 9H), 5.77 (d, 1H), 5.50 (bs, 1H), 4.83 (d, 1H), 3.36 (t, 2H), 2.72 (s, 3H), 2.46 (t, 2H), 2.39 (s, 3H), 2.20–2.05 (m, 1H), 1.96–1.75 (m, 1H), 1.74–1.40 (m, 2H), 0.63 (t, 3H); *m/z* 490 (MH⁺), C₂₇H₃₁N₅O₂S·0.5H₂O·HCl calculated C 60.60, H 6.22, N 13.09, Cl 6.63, found C 60.59, H 6.30, N 12.88, Cl 6.63.

Method 78. (+)-*N*-(3-Aminopropyl)-*N*-[1-(5-benzyl-3-methyl-4-oxo-[1,2]-thiazolo[5,4-*d*]pyrimidin-6-yl)propyl]-4-methylbenzamide Hydrochloride. (+)-*tert*-Butyl *N*-[3-[1-(5-benzyl-3-methyl-4-oxo-[1,2]-thiazolo[5,4-*d*]pyrimidin-6-yl)propyl-(4-methylbenzoyl)amino]propyl]carbamate (method 77) (0.117 g, 0.19 mmol) was dissolved in 2 M HCl in ether, and the mixture was stirred at rt for 20 h. The precipitated product was filtered off and washed with ether and dried in vacuo to yield the pure product (**68**) (91 mg, 87%): white powder, mp 127.8–129.2 °C; ¹H NMR (DMSO-*d*₆, 500 MHz, 96 °C) δ 0.63 (t, 3H), 1.40–1.74 (m, 2H), 1.75–1.96 (m, 1H), 2.05–2.20 (m, 1H), 2.39 (s, 3H), 2.46 (t, 2H), 2.72 (s, 3H), 3.36 (t, 2H), 4.83 (d, 1H), 5.50 (bs, 1H), 5.77 (d, 1H), 6.95–7.37 (m, 9H), 7.79 (bs, 3H); *m/z* 490 (MH⁺), C₂₇H₃₁N₅O₂S·1.55HCl calculated C 59.37, H 6.01, N 12.82, found C 59.39, H 6.45, N 12.38.

The following compounds were synthesized according to method 78:

(+)-*N*-(3-Aminopropyl)-*N*-[1-[5-[(4-fluorophenyl)methyl]-3-methyl-4-oxo-[1,2]-thiazolo[5,4-*d*]pyrimidin-6-yl]propyl]-4-methylbenzamide hydrochloride (**71**): ¹H NMR (DMSO-*d*₆, 500 MHz, 96 °C) δ 0.66 (t, 3H), 1.38–1.74 (m, 2H), 1.82–1.98 (m, 1H), 2.02–2.20 (m, 1H), 2.34 (s, 3H), 2.42 (t, 2H), 2.72 (s, 3H), 3.36 (t, 2H), 4.85 (d, 1H), 5.49 (bs, 1H), 5.70 (d, 1H), 7.05–7.27 (m, 8H), 7.76 (bs, 3H); *m/z* 508 (MH⁺), C₂₇H₃₀FN₅O₂S·3.25HCl calculated C 58.09, H 4.84, N 11.22, found C 58.09, H 5.49, N 12.19.

(+)-*N*-(3-Aminopropyl)-*N*-[1-[5-[(3-fluorophenyl)methyl]-3-methyl-4-oxo-[1,2]-thiazolo[5,4-*d*]pyrimidin-6-yl]propyl]-4-methylbenzamide hydrochloride (**73**): ¹H NMR (DMSO-*d*₆, 500 MHz, 100 °C) δ 0.70 (t, 3H), 1.40–1.54 (m, 1H), 1.62–1.76 (m, 1H), 1.85–2.01 (m, 1H), 2.14–2.27 (m, 1H), 2.38 (s, 3H), 2.44–2.49 (m, 2H), 2.76 (s, 3H), 3.35–3.46 (m, 2H), 4.87 (br s, 1H), 5.48 (br s, 1H), 5.75 (d, 1H), 6.84–6.96 (m, 2H), 7.06–7.15 (m, 1H), 7.20–7.31 (m, 4H), 7.33–7.41 (m, 1H),

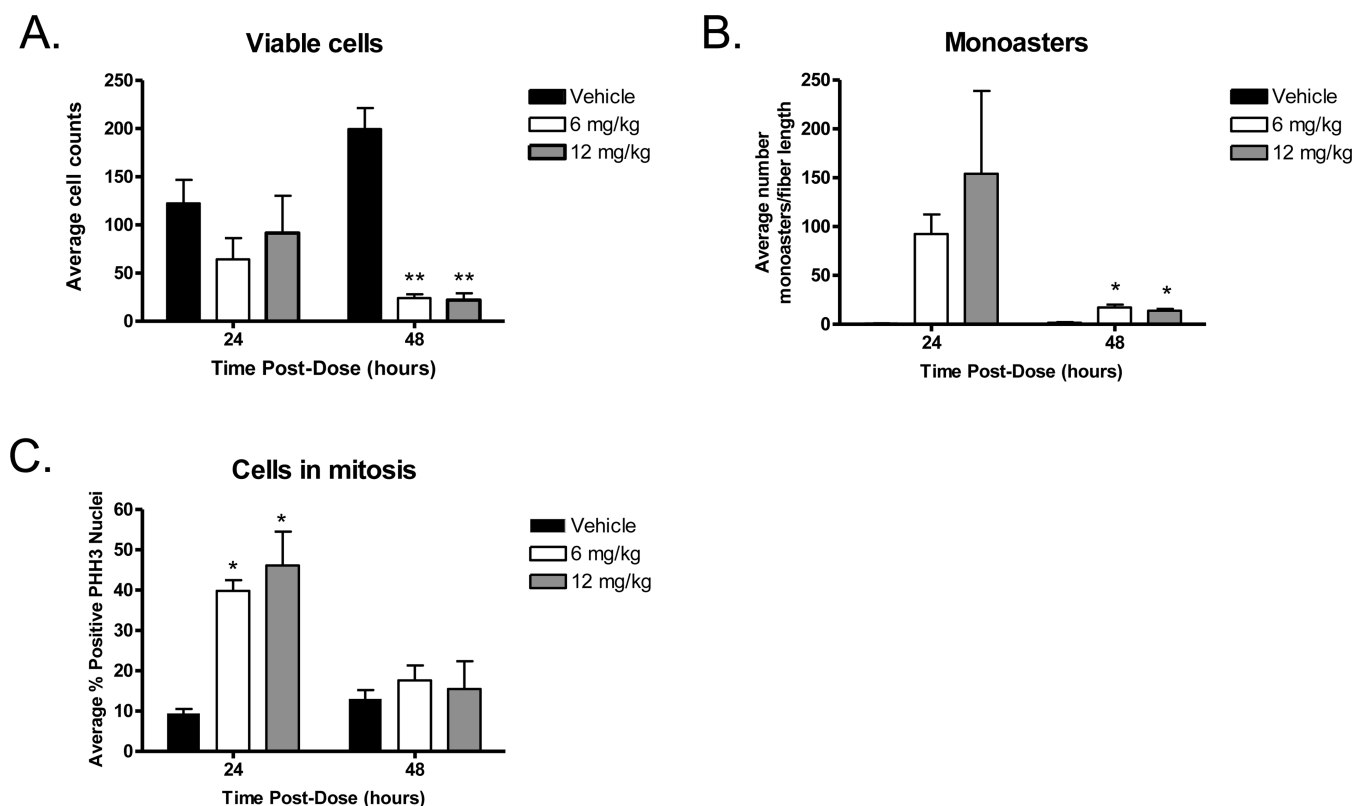


Figure 4. Compound 1 decreased cell viability, increased cells in mitosis and increased monoaster formation in a rat hollow fiber model. Viable cell counts (A), the number of monoasters (B), and percent phospho-histone-H3 (PHH₃) positive cells (C) obtained from sections of hollow fibers containing Colo205 cells. Sections were stained with either hematoxylin and eosin or antibodies that recognize α -tubulin and PHH₃, respectively. Fibers were removed from vehicle or compound 1 treated rats 24 and 48 h after administration of a single dose. Statistical analysis was performed using a standard Student *t* test (**p* < 0.05, ***p* < 0.01 compared to vehicle at same time point).

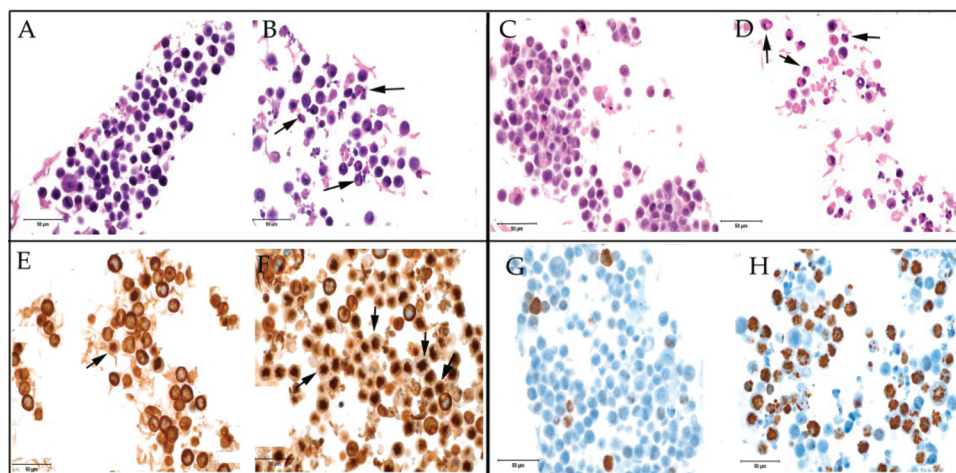


Figure 5. Effects of compound 1 on cell viability, monoaster formation and mitosis in hollow fibers. High power fields of view from sections of hollow fibers showing cell viability at 24 h (A, B) and 48 h (C, D), monoasters at 24 h (E, F), and cells in mitosis at 24 h (G, H). Sections were stained with either hematoxylin and eosin (A–D) or antibodies that recognize α -tubulin (E, F) and phospho-histone-H3 (G, H). Fibers were removed from vehicle (A, C, E, G) or 1 (B, D, F, H) treated rats 24 h (A, B, E–H) or 48 h (C, D) after administration of a single dose. Arrows indicate examples of cells undergoing cell death (B, D) or monoasters (E, F). Scale bar represents 50 μ m.

7.52 (br s, 3H); *m/z* 508 (MH⁺), C₂₇H₃₀FN₅O₂S·3.8HCl calculated C 57.24, H 4.68, N 10.84, found C 57.21, H 5.31, N 12.11.

(+)-*N*-(3-Aminopropyl)-*N*-[1-(5-benzyl-3-methyl-4-oxo-[1,2]thiazolo[5,4-*d*]pyrimidin-6-yl)propyl]-4-bromobenzamide hydrochloride (75): ¹H NMR (DMSO-*d*₆, 500 MHz, 96 °C) δ 0.68 (t, 3H), 1.50–1.72 (m,

2H), 1.91–1.96 (m, 1H), 2.13–2.17 (m, 1H), 2.47 (t, 2H), 2.77 (s, 3H), 3.38 (t, 2H), 4.95 (d, 1H), 5.57 (bs, 1H), 5.80 (d, 1H), 7.13 (m, 2H), 7.28–7.36 (m, 5H), 7.64 (d, 2H), 7.80 (br, 1H); *m/z* 554, 556 (MH⁺), C₂₆H₂₈BrN₅O₂S·2.8HCl calculated C 52.67, H 4.3, N 10.66, found C 52.69, H 5.36, N 9.39.

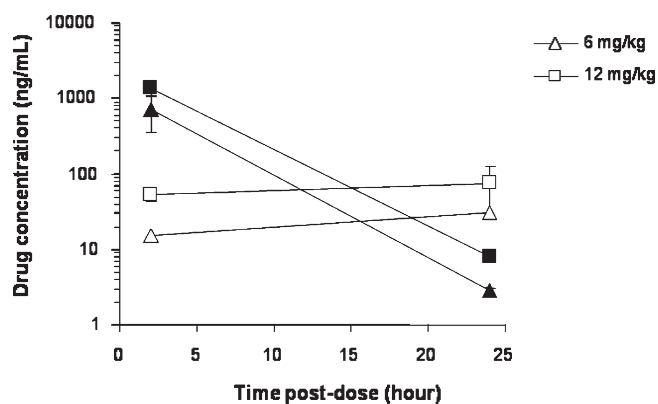


Figure 6. Exposure of compound **1** in rat plasma and hollow fibers. Samples were collected 2 and 24 h after administration of a single intravenous dose. Plasma drug concentration is shown in black and fiber concentration in white.

(+)-*N*-(3-Aminopropyl)-*N*-[1-(5-benzyl-3-methyl-4-oxo-[1,2]thiazolo[5,4-*d*]pyrimidin-6-yl)propyl]-3-fluoro-4-methylbenzamide hydrochloride (**77**): $^1\text{H NMR}$ (DMSO- d_6 , 500 MHz, 96 °C) δ 0.67 (t, 3H), 1.45 (m, 1H), 1.70 (m, 1H), 1.92 (m, 1H), 2.16 (m, 1H), 2.31 (s, 3H), 2.46 (2H, hidden by DMSO), 2.76 (s, 3H), 3.39 (t, 2H), 4.93 (d, 1H), 5.54 (bs, 1H), 5.81 (d, 1H), 7.09–7.52 (m, 8H), 7.74 (br, 3H); m/z 508 (MH^+); $\text{C}_{27}\text{H}_{30}\text{FN}_5\text{O}_2\text{S} \cdot 3.6\text{HCl}$ calculated C 57.52, H 4.73, N 10.96, found C 57.48, H 5.54, N 12.06.

Method 106. *N*-(3-Aminopropyl)-*N*-[1-(5-benzyl-3-methyl-4-oxo-[1,2]thiazolo[5,4-*d*]pyrimidin-6-yl)-2-methylpropyl]-4-methylbenzamide hydrochloride. *tert*-Butyl *N*-[3-[1-(5-benzyl-3-methyl-4-oxo-[1,2]thiazolo[5,4-*d*]pyrimidin-6-yl)-2-methylpropyl]-(4-methylbenzoyl)amino]propyl]-carbamate (method 104) (0.245 g, 0.40 mmol) was dissolved in 4 M HCl in 1,4-dioxane and the mixture was stirred at rt for 20 min. The reaction mixture was concentrated in a rotary evaporator, and the residue was triturated with ether. The precipitated product was filtered off, washed with ether and dried in vacuo to yield *N*-(3-aminopropyl)-*N*-[1-(5-benzyl-3-methyl-4-oxo-[1,2]thiazolo[5,4-*d*]pyrimidin-6-yl)-2-methylpropyl]-4-methylbenzamide as the hydrochloride salt (**65**) (0.219 g, 100%): white powder, mp 139–140 °C; $^1\text{H NMR}$ (DMSO- d_6 , 300 MHz, 96 °C) δ 0.45 (d, 3H), 0.90 (d, 3H), 1.12–1.30 (m, 1H), 1.46–1.63 (m, 1H), 2.25 (t, 2H), 2.36 (s, 3H), 2.64–2.7 (m, 1H), 2.68 (s, 3H), 3.34 (t, 2H), 5.06 (d, 1H), 5.59 (d, 1H), 5.90 (d, 1H), 7.20–7.40 (m, 9H), 7.71 (bs, 3H); m/z 504 (MH^+); $\text{C}_{28}\text{H}_{33}\text{N}_5\text{O}_2\text{S} \cdot 1\text{H}_2\text{O} \cdot 1.2\text{HCl}$, calculated C 59.48, H 6.45, N 12.39, Cl 7.52, found C 59.61, H 6.51, N 12.36, Cl 7.55.

The following compounds were synthesized according to method 106:

(+)-*N*-(3-Aminopropyl)-*N*-[1-(5-benzyl-3-methyl-4-oxo-[1,2]thiazolo[5,4-*d*]pyrimidin-6-yl)-2-methylpropyl]-4-methylbenzamide hydrochloride (**1**): $^1\text{H NMR}$ (500 MHz, 96 °C, DMSO- d_6) δ 0.45 (d, 3H), 0.90 (d, 3H), 1.12–1.30 (m, 1H), 1.46–1.63 (m, 1H), 2.25 (t, 2H), 2.36 (s, 3H), 2.64–2.7 (m, 1H), 2.68 (s, 3H), 3.34 (t, 2H), 5.06 (d, 1H), 5.59 (d, 1H), 5.90 (d, 1H), 7.20–7.40 (m, 9H), 7.71 (bs, 3H); m/z 504 (MH^+); $\text{C}_{28}\text{H}_{33}\text{N}_5\text{O}_2\text{S} \cdot 1\text{H}_2\text{O} \cdot 1\text{HCl}$ calculated C 60.26, H 6.50, N 12.55, found C 60.20, H 6.28, N 12.40.

(+)-*N*-(3-Aminopropyl)-*N*-[1-[5-[(4-fluorophenyl)methyl]-3-methyl-4-oxo-[1,2]thiazolo[5,4-*d*]pyrimidin-6-yl)-2-methylpropyl]-4-methylbenzamide hydrochloride (**72**): $^1\text{H NMR}$ (500 MHz, 90 °C, DMSO- d_6) δ 0.47 (d, 3H), 0.92 (d, 3H), 1.10–1.28 (m, 1H), 1.44–1.56 (m, 1H), 2.27 (t, 2H), 2.36 (s, 3H), 2.66–2.72 (m, 1H), 2.75 (s, 3H), 3.35 (t, 2H), 5.04 (d, 1H), 5.57 (d, 1H), 5.86 (d, 1H), 7.12–7.43 (m, 8H), 7.71–7.81 (m, 3H); m/z 522 (MH^+); $\text{C}_{28}\text{H}_{32}\text{FN}_5\text{O}_2\text{S} \cdot 4\text{HCl}$ calculated C 57.57, H 4.83, N 10.49, found C 57.53, H 5.70, N 11.22.

(+)-*N*-(3-Aminopropyl)-*N*-[1-[5-[(3-fluorophenyl)methyl]-3-methyl-4-oxo-[1,2]thiazolo[5,4-*d*]pyrimidin-6-yl)-2-methylpropyl]-4-methylbenzamide hydrochloride (**74**): $^1\text{H NMR}$ (500 MHz, 90 °C, DMSO- d_6)

δ 0.52 (d, 3H), 0.94 (d, 3H), 1.15–1.25 (m, 1H), 1.26–1.33 (m, 1H), 1.45–1.58 (m, 1H), 2.32 (m, 2H), 2.38 (s, 3H), 2.78 (s, 3H), 3.32–3.40 (m, 2H), 5.11 (bd, 1H), 5.56 (bd, 1H), 5.90–5.93 (d, 1H), 7.11–7.38 (m, 8H), 7.58 (b, 2H); m/z 522 (MH^+); $\text{C}_{28}\text{H}_{32}\text{FN}_5\text{O}_2\text{S} \cdot 2.3$ dioxane $\cdot 2\text{HCl}$ calculated C 56.05, H 6.63, N 8.78, found C 55.42, H 6.45, N 8.77.

(+)-*N*-(3-Aminopropyl)-*N*-[1-(5-benzyl-3-methyl-4-oxo-[1,2]thiazolo[5,4-*d*]pyrimidin-6-yl)-2-methylpropyl]-4-bromobenzamide hydrochloride (**76**): $^1\text{H NMR}$ (500 MHz, 90 °C, DMSO- d_6) δ 0.48 (d, 3H), 0.93 (m, 3H), 1.10–1.20 (m, 1H), 1.45–1.60 (m, 1H), 2.28–2.41 (t, 2H), 2.63–2.79 (m, s, 4H), 3.35–3.43 (m, 2H), 5.08 (m, 1H), 5.62 (m, 1H), 5.96 (d, 1H), 7.30–7.50 (m, 7H), 7.52–7.80 (br, m, 4H); m/z 568, 570 (MH^+); $\text{C}_{27}\text{H}_{30}\text{BrN}_5\text{O}_2\text{S} \cdot 4\text{HCl}$ calculated C 52.11, H 4.23, N 9.8, found C 51.91, H 5.08, N 10.99.

(+)-*N*-(3-Aminopropyl)-*N*-[1-(5-benzyl-3-methyl-4-oxo-[1,2]thiazolo[5,4-*d*]pyrimidin-6-yl)-2-methylpropyl]-3-fluoro-4-methylbenzamide hydrochloride (**78**): $^1\text{H NMR}$ (500 MHz, 90 °C, DMSO- d_6) δ 0.48 (d, 3H), 0.93 (d, 3H), 1.18 (m, 1H), 1.53 (m, 1H), 2.32–2.51 (s, m, 5H), 2.82 (s, 4H), 3.35–3.43 (m, 2H), 5.10 (m, 1H), 5.62 (m, 1H), 5.94 (d, 1H), 7.11–7.38 (m, 8H), 7.51 (b, 2H); m/z 522 (MH^+); $\text{C}_{27}\text{H}_{31}\text{N}_5\text{O}_2\text{S} \cdot 3.7\text{HCl}$ calculated C 57.98, H 4.91, N 10.66, found C 58.00, H 5.92, N 11.95.

Enzyme IC_{50} Determination (Eg5 ATPase). The ability of compounds to inhibit Eg5 ATPase activity was examined using a malachite green assay with recombinant Eg5 (human Eg5 N-terminal 369 amino acids with a C-terminal 8 histidine tag; 0.4 nM), polymerized microtubules (0.1 mg/mL) and a nonsaturating concentration of adenosine-5'-triphosphate (ATP) (75 μM). In brief, C-terminal His6-tagged recombinant protein was expressed in bacteria and purified using nickel-nitrilotriacetic acid (Ni-NTA) affinity chromatography. Purified protein and polymerized microtubules in a piperazine-*N,N'*-bis(2-ethanesulfonic acid (PIPES) based buffer (pH 6.8) were added to a 384-well plate containing diluted compound (final 11-point concentration range from 100 μM to 1.7 nM). Reactions were initiated by the addition of enzyme/microtubule mixture, and plates were allowed to incubate for 1 h at room temperature (24 °C). Reactions were then quenched with malachite green reagent and read at A650 after 10 min in a microplate reader. IC_{50} was determined using XLFit within Activity Base.

Enzyme IC_{50} Determination (Conventional Kinesin ATPase). Compound inhibition of conventional kinesin ATPase activity was examined following the Eg5 malachite green assay protocol with several changes. A 20 min assay was performed with 3 nM recombinant kinesin (glutathione *S*-transferase (GST) tagged human kinesin heavy chain motor protein; Cytoskeleton catalog no. KR01), 0.6 mg/mL polymerized microtubules and 300 μM ATP. Compound inhibition of MKLP1 ATPase activity was also examined following the Eg5 malachite green assay protocol with several changes. A 20 min assay was performed with 10 nM recombinant MKLP1 (GST-human MKLP1 Kinesin motor domain; Cytoskeleton catalog no. MP01), 0.15 mg/mL polymerized microtubules and 300 μM ATP.

Cellular IC_{50} Determination. Colo205 cells were plated in 96-well flat bottomed plates at a density of 3.3×10^4 cells per well. After an initial 24 h period in culture, a predose plate was read to establish baseline. Remaining cell plates were treated in triplicate with compounds (using a 9-point concentration range from 10 μM to 0.3 nM + DMSO control) and left for an additional 72 h. Cell proliferation was evaluated by the MTS assay, according to the manufacturer's instructions (Promega, Madison, WI, p/n G3581; 3-(4,5-dimethylthiazol-2-yl)-5-(3-carboxymethoxyphenyl)-2-(4-sulfophenyl)-2H-tetrazolium (MTS), in the presence of phenazine methosulfate (PMS), produces a formazan product that has an absorbance maximum at 490–500 nm in phosphate-buffered saline).

Solubility Determination. Equilibrium solubility was determined in aqueous buffer at pH 7.4. The compounds were serially diluted in 0.1 M pH 7.4 phosphate buffer at 25 °C with agitation for 24 h. Undissolved material was removed by filtration, and the filtrates were quantitated

against a standard in DMSO prepared from the same DMSO stock using a generic HPLC–UV method with mass spectroscopy mass confirmation.

Animals. Hans Wistar rats were purchased from Charles River. All procedures were conducted in accordance with the Institute for Laboratory Animal Research Guide for the Care and Use of Laboratory Animals and within the protocols approved by the Institute of Animal Care and Use Committee at AstraZeneca.

Rat Hollow Fiber Model. Fibers made from polyvinylidene difluoride (molecular weight cutoff, 500 kDa; Spectrum) were immersed in 70% ethanol for 72 h, flushed with distilled water, and autoclaved. Colo205 cells (obtained from American Type Culture Collection) were suspended in Roswell Park Memorial Institute (RPMI) medium with 20% fetal bovine serum and loaded into the fibers (5×10^6 cells/mL) and the fibers sealed at both ends. Following overnight incubation in media at 37 °C, fibers were implanted subcutaneously into rats. After several hours, a single dose of 1 or vehicle (sterile saline) was administered over approximately 1 min through a jugular vein cannula (3 rats per treatment group). Fibers and plasma were collected at 2, 24, or 48 h after treatment and processed for either histology/immunohistochemistry (IHC) or drug exposure analysis (1 fiber per time-point per assay).

Histology/Immunohistochemistry (IHC). Formalin fixed paraffin embedded sections were prepared from the fibers and placed onto slides. Hematoxylin and eosin staining was performed on a Sakura 2000 autostainer. In brief, the slides were deparaffinized, hydrated, stained in Gill #2 hematoxylin (Polysciences Inc.), rinsed in water, blued in Lerner Bluing reagent (Fisher) and counterstained in Eosin Y (Shandon). Alpha tubulin and PHH₃ immunostaining were performed on a Ventana Discovery XT Immunostainer. Slides were incubated in the primary PHH₃ antibody (CST-9601, Cell Signaling Technology) at a 1:50 dilution followed by detection with a biotinylated goat anti-rabbit secondary antibody (PK-6101, Vector Laboratories). Slides were incubated in the primary α -tubulin antibody (Sigma T9026) at a 1:20,000 dilution followed by detection with a biotinylated mouse secondary antibody (Vector, PK-6102). Secondary antibodies were detected with a Ventana DABMap kit (Ventana cat. no. 760-124; (DAB refers to 3,3'-diaminobenzidine)). Slides were then counterstained with hematoxylin (Ventana 760-2021) and blued with bluing reagent (Ventana 760-2037) before being dehydrated, cleared and mounted.

A pathologist reviewed all slides. For each stain, 4–6 serial sections were examined from each paraffin block. The number of viable cells was determined from hematoxylin and eosin stained sections by manually counting cells from 3 high power (200 \times) fields of view for every fiber section. The percent PHH₃ positive nuclei was obtained by dividing the number of PHH₃ positive nuclei by total nuclei. Counts of positive nuclei and total nuclei were determined for every fiber section using Aperio Image analysis software. Fiber sections with fewer than 10 total nuclei were excluded from the analysis. Monoasters were examined on α -tubulin stained sections and counted manually. The number of monoasters per fiber length was obtained by dividing the total number of monoasters for every fiber section by the fiber length (cm).

■ ASSOCIATED CONTENT

Supporting Information. Extensive experimental procedures for the preparation of all compounds, including spectral data assignments. This material is available free of charge via the Internet at <http://pubs.acs.org>.

■ AUTHOR INFORMATION

Corresponding Author

*E-mail: Maria-Elena.Theoclitou@astrazeneca.com. Tel: 0044 (1) 625 233157.

Present Addresses

^{||}Lilly Corporate Centre, Indianapolis, Indiana 46285, United States.

[†]Memorial Sloan-Kettering Cancer Centre, 1272 York Avenue, New York, New York 10065, United States.

Notes

[§]Previously AstraZeneca Boston.

[#]Previous employees of Organix Inc., 240 Salem St., Woburn, Massachusetts 01801, United States.

■ ACKNOWLEDGMENT

We thank Nancy DeGrace for determining chiral separation conditions for all compounds mentioned.

■ ABBREVIATIONS USED

APCI, atmospheric pressure chemical ionization; ATP, adenosine-5'-triphosphate; CDCl₃, deuterated chloroform; CI, chemical ionization; CYP450, cytochrome P450; DAB, 3,3'-diaminobenzidine; EI, electron impact; ESP, electrospray; GST, glutathione S-transferase; HsEg5, *Homo sapiens* Eg5; IHC, immunohistochemistry; iv, intravenous; KSP, kinesin spindle protein; LC, liquid chromatography; LCK, lymphocyte specific protein tyrosine kinase; MAPKAP-K1a, mitogen-activated protein kinase-activated protein kinase 1a; MKLP, mitotic kinesin-like protein; MTS, 3-(4,5-dimethylthiazol-2-yl)-5-(3-carboxymethoxyphenyl)-2-(4-sulfophenyl)-2H-tetrazolium; MSD, mass spectroscopy detector; Ni-NTA, nickel-nitrilotriacetic acid; PHH₃, phosphohistone-H3; PIPES, piperazine-*N,N'*-bis(2-ethanesulfonic acid); PMS, phenazine methosulfate; RPMI, Roswell Park Memorial Institute; TMS, tetramethylsilane

■ REFERENCES

- (1) Rowinski, E. K.; Onetto, N.; Canetta Renzo, M.; Arbuck, S. G. Taxol: the first of the taxanes, an important new class of antitumor agents. *Semin. Oncol.* **1992**, *19*, 646–662.
- (2) Chabner, B. A.; Ryan, D. P.; Paz-Ares, L.; Garcia-Carbonero, R.; Calabresi, P. Antineoplastic agents. In *Goodman and Gilman's The Pharmacological Basis of Therapeutics*, 10th ed.; Hardman, J. G., Limbird, L. E., Gilman, A. G., Eds.; The McGraw-Hill Companies, Inc.: 2001.
- (3) Blagosklonny, M. V.; Fojo, T. Molecular effects of paclitaxel: myths and reality (a critical review). *Int. J. Cancer* **1999**, *83*, 151–156.
- (4) Samson, F. E., Jr. Mechanism of axoplasmic transport. *J. Neurobiol.* **1971**, *2*, 347–360.
- (5) Chan, S. Y.; Worth, R.; Ochs, S. Block of axoplasmic transport in vitro by *Vinca* alkaloids. *J. Neurobiol.* **1980**, *11*, 251–264.
- (6) Orr, G. A.; Verdier-Pinard, P.; McDaid, H. M.; Horwitz, S. B. Mechanisms of Taxol Resistance Related to Microtubules. *Oncogene* **2003**, *22*, 7280–7295.
- (7) Gottesman, M. M. Mechanisms of cancer drug resistance. *Annu. Rev. Med.* **2002**, *53*, 615–627.
- (8) Jordan, M. A.; Wilson, L. Microtubules as target for anticancer drugs. *Nat. Rev. Cancer* **2004**, *4*, 253–265.
- (9) Sablin, E. P. Kinesins and microtubules: their structures and motor mechanisms. *Curr. Opin. Cell. Biol.* **2000**, *12*, 35–41. Schief, W. R.; Howard, J. Conformational changes during kinesin motility. *Curr. Opin. Cell. Biol.* **2001**, *13*, 19–28.
- (10) Blangy, A.; Lane, H. A.; d'Herin, P.; Harper, M.; Kress, M.; Nigg, E. A. Phosphorylation by p34cdc2 regulates spindle association of human Eg5, a kinesin-related motor essential for bipolar spindle formation in vivo. *Cell* **1995**, *83*, 1159–1169.
- (11) Ferhat, L.; Cook, C.; Chauviere, M.; Muriel, C.; Harper, M.; Kress, M.; Lyons, G. E.; Baas, P. W. Expression of the Mitotic Motor

Protein Eg5 in Postmitotic Neurons: Implications for Neuronal Development. *J. Neurosci.* **1998**, *18* (19), 7822–7835.

(12) Sawin, K. E.; LeGuellec, K.; Philippe, M.; Mitchison, T. J. Mitotic spindle organization by a plus-end-directed microtubule motor. *Nature* **1992**, *359*, 540–543.

(13) Kashina, A. S.; Rogers, G. C.; Scholey, J. M. The bimC family of kinesins: essential bipolar mitotic motors driving centrosome separation. *Biochem. Biophys. Acta* **1997**, *1357*, 257–271.

(14) LeGuellec, R.; Paris, J.; Couturier, A.; Roghi, C.; Philippe, M. Cloning by differential screening of a *Xenopus* cDNA that encodes a kinesin-related protein. *Mol. Cell. Biol.* **1991**, *11*, 3395–3398.

(15) Heck, M. M. S.; Pereira, A.; Pesavento, P.; Yannoni, Y.; Spradling, A. C.; Goldstein, L. S. B. The kinesin-like protein KLP61F is essential for mitosis in *Drosophila*. *J. Cell Biol.* **1993**, *123*, 665–679.

(16) Castillo, A.; Morse, H. C.; Godfrey, V. L.; Naeem, R.; Justice, M. J. Overexpression of Eg5 causes genomic instability and tumor formation in mice. *Cancer Res.* **2007**, *67*, 10138–10147.

(17) Walczak, C. E.; Vernos, I.; Mitchison, T. J.; Karsenti, E.; Heald, R. A model for the proposed roles of different microtubule-based motor proteins in establishing spindle bipolarity. *Curr. Biol.* **1998**, *8*, 903–913.

(18) Mayer, T. U.; Kapoor, T. M.; Haggarty, S. J.; King, R. W.; Schreiber, S. L.; Mitchison, T. J. Small molecule inhibitor of mitotic spindle bipolarity identified in a phenotype-based screen. *Science* **1999**, *286*, 971–974.

(19) Jackson, J. R.; Patrick, D. R.; Dar, M. M.; Huang, P. S. Targeted anti-mitotic therapies: can we improve on tubulin agents? *Nat. Rev. Cancer* **2007**, *7*, 107–117.

(20) Hegde P. S.; Cogswell J.; Carrick K.; Jackson J.; Wood K. W.; Eng W. K.; Brawner M.; Huang P. S.; Bergsma D. Differential gene expression analysis of kinesin spindle protein in human solid tumors. *Proc. Am. Soc. Clin. Oncol.* **2003**, *22*, abstract 535.

(21) Carter, B. Z.; Mak, D. H.; Shi, Y.; Schoeber, W. D.; Wang, R. Y.; Konopleva, M.; Koller, E.; Dean, N. M.; Andreeff, M. Regulation and targeting of Eg5, a mitotic motor protein in blast crisis CML: overcoming imatinib resistance. *Cell Cycle* **2006**, *5*, 2223–2229.

(22) Hansen, G. M.; Justice, M. J. Activation of Hex and mEg5 by retroviral insertion may contribute to mouse B-cell leukemia. *Oncogene* **1999**, *18*, 6531–6539.

(23) Finer J. T.; Bergnes G.; Feng B.; Smith W.; Chabala J. C. PCT Publ., 2001, WO 01/30768.

(24) Fraley M. E.; Hartman G. D. PCT Publ., 2003, WO 03/050122, WO 03/039460, WO 03/050064, WO 03/049678, WO 03/049679, WO 03/049527.

(25) Hackney, D. D.; Jiang, W. Assays for kinesin microtubule-stimulated ATPase activity. *Methods Mol. Biol.* **2001**, *164*, 65–71.

(26) Sorbera, L. A.; Bolos, J.; Serradell, N.; Bayes, M. Ispinesib mesilate. *Drugs Future* **2006**, *31*, 778–787.

(27) Cox, C. D.; Breslin, M. J.; Mariano, B. J.; Coleman, P. J.; Buser, C. A.; Walsh, E. S.; Hamilton, K.; Huber, H. E.; Kohl, N. E.; Torrent, M.; Yan, Y.; Kuo, L. C.; Hartman, G. D. Kinesin spindle protein (KSP) inhibitors. Part 1: The discovery of 3,5-diaryl-4,5-dihydropyrazoles as potent and selective inhibitors of the mitotic kinesin KSP. *Bioorg. Med. Chem. Lett.* **2005**, *15*, 2041–2045.

(28) Marcus, A. I.; Peters, U.; Thomas, S. L.; Garrett, S.; Zelnak, A.; Kapoor, T. M.; Giannakakou, P. Mitotic kinesin inhibitors induce mitotic arrest and cell death in taxol-resistant and -sensitive cancer cells. *J. Biol. Chem.* **2005**, *280*, 11569–11577.

(29) Bergnes, G.; Brejc, K.; Belmont, L. Mitotic Kinesins: Prospects for Antimitotic Drug Discovery. *Curr. Top. Med. Chem.* **2005**, *5*, 127–145.

(30) Sakowicz, R.; Finer, J. T.; Beraud, C.; Crompton, A.; Lewis, E.; Fritsch, A.; Lee, Y.; Mak, J.; Moody, R.; Turincio, R.; Chabala, J. C.; Gonzales, P.; Roth, S.; Weitman, S.; Wood, K. W. Antitumor activity of a kinesin inhibitor. *Cancer Res.* **2004**, *64*, 3276–3280.

(31) Hotha, S.; Yarrow, J. C.; Yang, J. G.; Garrett, S.; Renduchintala, K. V.; Mayer, T. U.; Kapoor, T. M. HR22C16: a potent small-molecule probe for the dynamics of cell division. *Angew. Chem., Int. Ed.* **2003**, *30* (42), 2379–2382.

(32) Cox, C. D.; Coleman, P. J.; Breslin, M. J.; Whitman, D. B.; Garbaccio, R. M.; Fraley, M. E.; Buser, C. A.; Walsh, E. S.; Hamilton, K.; Schaber, M. D.; Lobell, R. B.; Tao, W.; Davide, J. P.; Diehl, R. E.; Abrams, M. T.; South, V. J.; Huber, H. E.; Torrent, M.; Prueksaranant, T.; Li, C.; Slaughter, D. E.; Mahan, E.; Fernandez-Metzler, C.; Yan, Y.; Kuo, L. C.; Kohl, N. E.; Hartman, G. D. Kinesin Spindle Protein (KSP) Inhibitors. 9. Discovery of (2S)-4-(2,5-Difluorophenyl)-N-[(3R,4S)-3-fluoro-1-methylpiperidin-4-yl]-2-(hydroxymethyl)-N-methyl-2-phenyl-2,5-dihydro-1H-pyrrole-1-carboxamide (MK-0731) for the Treatment of Taxane-Refractory Cancer. *J. Med. Chem.* **2008**, *51*, 4239–4252.

(33) Bergnes G.; Ha E.; Feng B.; Smith W. W.; Yao B.; Tochimoto T.; Lewis E. R.; Lee Y.; Moody R. S.; Finer J. T.; Turinci R. A.; Wood K.; Sakowicz R.; Crompton A. M.; Chabala J. C.; Morgans D. J.; Sigal N. H.; Sabry J. H. Mitotic kinesin-targeted antitumor agents: Discovery, lead optimization and anti-tumor activity of a series of novel quinazolinones as inhibitors of kinesin spindle protein (KSP). In *Abstracts of Papers*, 223rd National Meeting of the American Chemical Society, Orlando, FL, United States; American Chemical Society: Washington, DC, 2002; MEDI-249.

(34) McDonald A.; Bergenes G.; Feng B.; Morgans D. J. C.; Knight S. D.; Newlander K. A.; Dhanak D.; Brook C. S. PCT Publ., 2003, WO 03/088903.

(35) DeBonis, S.; Skoufias, D. A.; Lebeau, L.; Lopez, R.; Robin, G.; Margolis, R. L.; Wade, R. H.; Kozielski, F. In vitro screening for inhibitors of the human mitotic kinesin Eg5 with antimitotic and antitumor activities. *Mol. Cancer Ther.* **2004**, *3*, 1079–1090.

(36) Hans J.; Wallace E. M.; Zhao Q.; Lyssikatos J. P.; Aicher T.; Laird E.; Robinson J.; Allen S. PCT Publ., 2006, WO 06/044825

(37) Ahrendt K.; Delisle R. K.; Hans J.; Lyssikatos J. P.; Robinson J.; Wallace E. M.; Zhao Q.; PCT Publ., 2008, WO 08/042928.

(38) Chin, G. M.; Herbst, R. Induction of apoptosis by monastrol, an inhibitor of the mitotic kinesin Eg5, is independent of the spindle checkpoint. *Mol. Cancer Ther.* **2006**, *5*, 2580–2591.

(39) Woessner R.; Corrette C.; Allen S.; Hans J.; Zhao Q.; Aicher T.; Lyssikatos J.; Robinson J.; Poch G.; Hayter L.; Cox A.; Lee P.; Winkler J.; Koch K.; Wallace E. ARRY-520: a KSP inhibitor with efficacy and pharmacodynamic activity in animal models of solid tumors. AACR Annual Meeting, 2007.

(40) Lemieux C.; DeWolf W.; Voegtli W.; DeLisle R. K.; Laird E.; Wallace E.; Woessner R.; Corrette C.; Allen S.; Hans J.; Zhao Q.; Aicher T.; Lyssikatos J.; Robinson J.; Koch K.; Winkler J.; Gross S. ARRY-520: a novel, highly selective KSP inhibitor with potent anti-proliferative activity. AACR Annual Meeting, 2007.

(41) Aquila B.; Block, M. H.; Davies, A.; Ezhuthachan, J.; Filla, S.; Luke, R.; Pontz, T.; Theoclitou, M. E.; Zheng, X; PCT Int. Appl., 2004, WO 04/078758

(42) Block M. H.; Davies A.; Russell D.; Theoclitou M. E.; PCT Int. Appl., 2006, WO 06/008523

(43) Finer J. T.; Bergnes G.; Feng B.; Smith W. W.; Chabala J.; PCT Publ., 2001, WO 01/30768 A1

(44) Kantarjian H. M.; Padmanabhan S.; Stock W.; Tallman M. S.; Curt G. A.; Li J.; Osmukhina A.; Wu K.; Huszar D.; Borthukar G.; Faderl S.; Garcia-Manero G.; Kadia T.; Sankhala K.; Odenike O.; Altman J. K.; Minden M. Phase I/II multicenter study to assess the safety, tolerability, pharmacokinetics and pharmacodynamics of AZD4877 in patients with refractory acute myeloid leukemia. *Invest. New Drugs*, **2011**, published online.